The mechanical properties of multi-scale metallic materials

Chapter · March 2011

DOI: 10.1533/9780857091123.3.375

Yonghao Zhao
Nanjing University of Science and Technology

13

The mechanical properties of multi-scale metallic materials

Y.H. ZHAO and E.J. LAVERNIA,
University of California Davis, USA

Abstract: Bulk nanostructured metallic materials with a multi-scale grain size distribution possess both high strength and good ductility, and therefore are expected to have important technological implications. This chapter introduces the basic concepts of bulk multi-scale, bimodal and multimodal metallic materials and discusses their development background and preparation methods, followed by a review of the experimental and numerical results of mechanical properties (primarily strength and ductility), and deformation and fracture mechanisms of bimodal and multimodal metallic materials, and ends with a final discussion on the potential technological impact and future work.

Key words: bulk multi-scale metallic materials, bimodal and multimodal metallic materials, strength and ductility, deformation and fracture mechanisms.

13.1 Introduction

In the case of polycrystalline materials, such as metals, alloys, ceramics and intermetallics, grain size (i.e. fraction of grain boundary volume) is one of the most important microstructural parameters that influence properties and deformation mechanisms. For instance, the mean grain size generally influences the low-temperature yield strength of polycrystals via the well-known Hall–Petch relationship. The grain size of conventional structural polycrystalline materials typically falls in what is widely described as the coarse-grained (CG) regime (>1 µm, see Fig. 13.1) which may include the fine-grained sub-regime (1–10 µm).[1] Over the past couple of decades, nanocrystalline (or bulk nanostructured, <100 nm)[2] and ultrafine-grained (UFG, <1 µm)[3] metallic materials have emerged as a new class of materials and have been the subject of widespread research studies. By extending the grain size down to the nanometer regime (see Fig. 13.1), UFG materials provide us not only with an excellent opportunity to study structure–property relationships in polycrystalline materials, but also present us with an attractive potential for technological applications with their novel properties. Initially, fundamental interest in this class of materials was motivated by the question of whether the large volume fraction of grain boundaries (GBs, 50% for 5 nm grains, 30% for 10 nm grains) in UFG metallic materials will significantly alter their physical, mechanical and chemical properties in comparison

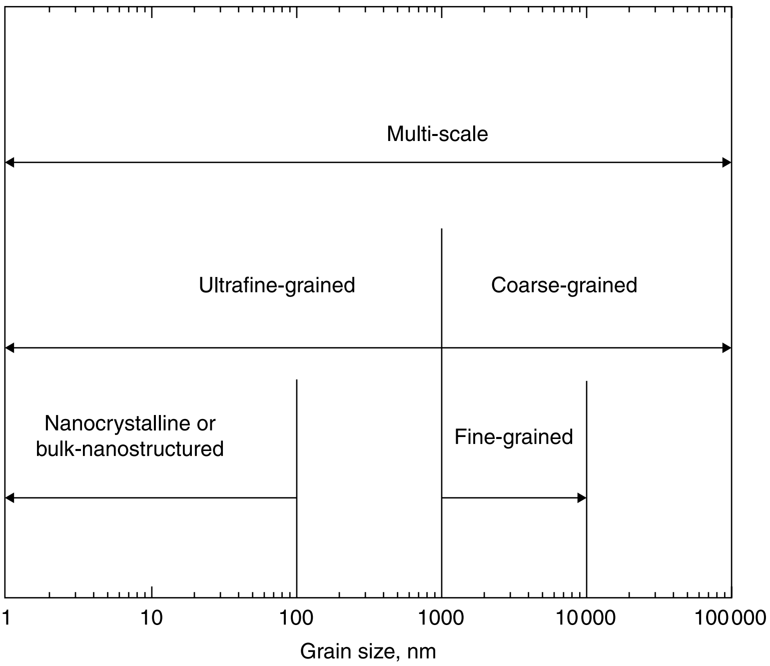

13.1 Grain size regimes of nanocrystalline, fine-grained, ultrafine-grained, coarse-grained and multi-scale metallic materials.

with those of conventional CG metallic materials. For instance, with the validity of extending the Hall–Petch relationship down to at least a small threshold grain size value of about 10–20 nm,[4] the strength of UFG metallic materials is typically 5–10 times that of conventional CG material of similar composition, and thus offers interesting possibilities related to structural applications.

In the case of structural metallic materials, strength and ductility are two of the most important mechanical properties. A structure must support load, thus mechanical strength is an obvious requirement and quite often it is among the most important criteria of any metallic materials selection decision. In addition, good ductility is essential to avoid catastrophic failure in load-bearing applications and for many shaping and forming operations without tearing or fracturing. Ductility is usually defined as the extent to which a material can be deformed plastically and measured in uniaxial tension. It is desirable that structural metallic materials have both high strength and high ductility. However, strength and ductility are often achieved at a trade-off, i.e. increasing the strength sacrifices the ductility, and elevating the ductility typically lowers the strength. This strength–ductility dilemma also applies to CG and UFG metals and alloys: the former have good ductility but low strength, while the latter have high strength but low ductility.[5] The low tensile ductility in UFG metallic materials can be attributed to the premature onset of plastic instability (necking), which is further caused by low strain-hardening capability.[6] According to Considère's criterion,[7] strain hardening is required in order to delay the initiation of tensile necking. Strain hardening typically results from the interactions of dislocations as they glide and intersect with each other. Typically, CG grains provide adequate spacing for significant numbers of dislocation intersections during deformation, while in UFG grains, dislocations move and accumulate at opposing GBs directly, and thereby result in minimal hardening.[4]

Low ductility has become a seemingly insurmountable obstacle for the widespread technological applications of UFG metallic materials. Since the year 2000, many efforts have been put forth to develop strategies for improving poor ductility.[8–12] For CG metallic materials, the ductility and yielding, as well as the working hardening behavior, is generally insensitive to the character of the grain size distribution, such as the Hall–Petch relationship that references only the mean grain size distribution. However, for UFG metallic materials, the grain size distribution becomes potentially more important so that there exists the opportunity for manipulating the grain size distribution to control mechanical behavior. With such a background, bulk multi-scale metallic materials were originally developed as an important strategy for ductility enhancement of UFG metallic materials. Bulk multi-scale metallic materials usually have a wide grain size distribution ranging from the UFG to the CG regions (Fig. 13.1). The grain size distribution histogram could have either a two-peak feature or a continuous log-normal feature, where the former distribution is terminated by a bimodal grain size distribution and the latter by a multimodal grain size distribution. Figure 13.2 (a) shows a transmission electron microscopy (TEM) image of Cu with a bimodal grain size distribution, prepared by dynamic plastic deformation (DPD) and a subsequent annealing treatment.[13] Two grain size distribution peaks are observed: the peak at small grain size values, ranging from about 20 to 200 nm with a mean value of about 75 nm, corresponds to the as-deformed nanocrystalline Cu matrix, and the peak at large grain size values, ranging from 1 to 6 μm with a mean value of 2.2 μm, represents the CG grains formed by a secondary recrystallization (Fig. 13.2 (b)). Figure 13.3 shows an electron backscattering diffraction (EBSD) crystal orientation mapping and corresponding grain size distribution histogram for multimodal Ni prepared by cryomilling and powder consolidation.[14] The grain size has a log-normal distribution ranging from about 100 nm to 10 μm and the mean grain size is about 1 μm.

The increasing importance of grain size distribution for multi-scale metallic materials can be examined in terms of two competing effects. First, the UFG grains at the small end of the size distribution possess increasingly higher strength relative to their larger counterparts. Conversely, the CG grains at the large end of the distribution occupy a larger proportion of the microstructure on a volumetric basis, thus increasing their effect on the behavior of the aggregate, such as ductility. Thus, the multi-scale metallic materials have a good combination of

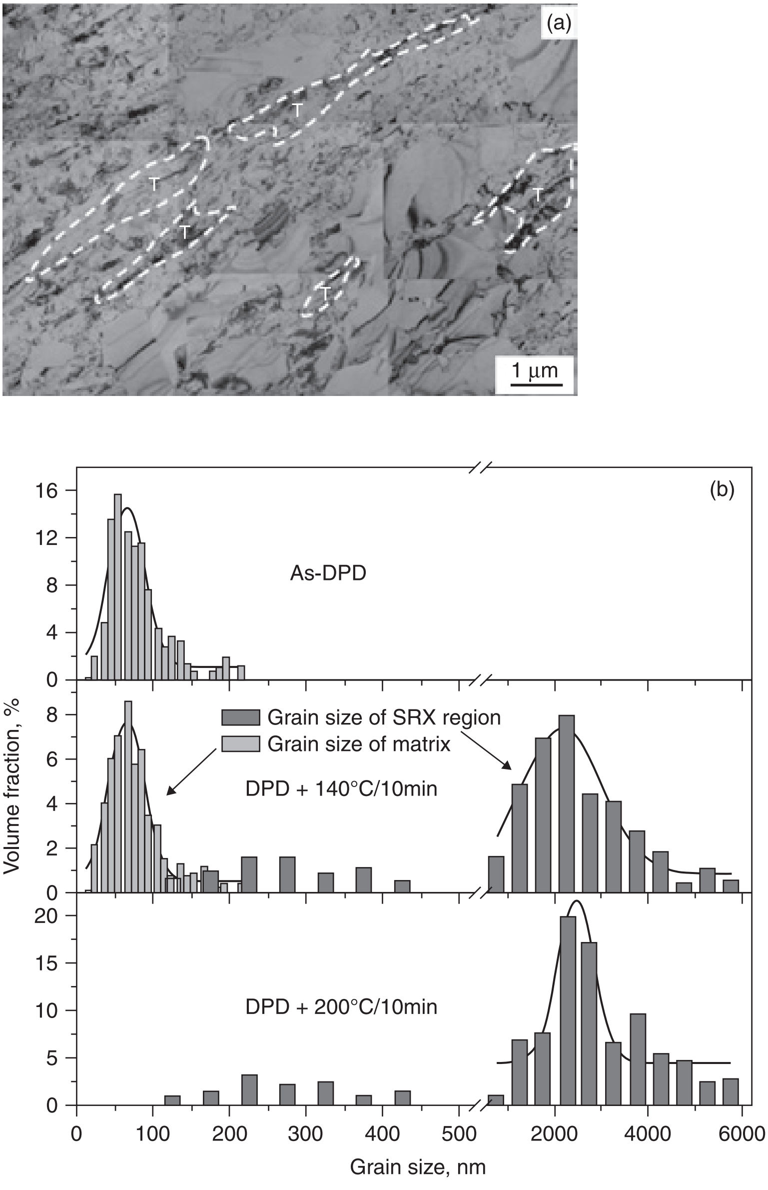

13.2 (a) Bright-field transmission electron microscopy (TEM) image of a bimodal Cu sample annealed at 140°C for 10 min. The recrystallized coarse grains are surrounded by areas of nanograins and remaining nanotwin bundles outlined and labeled "T". (b) Grain size distributions of the as-DPD Cu sample and as-annealed bimodal Cu samples.[13]

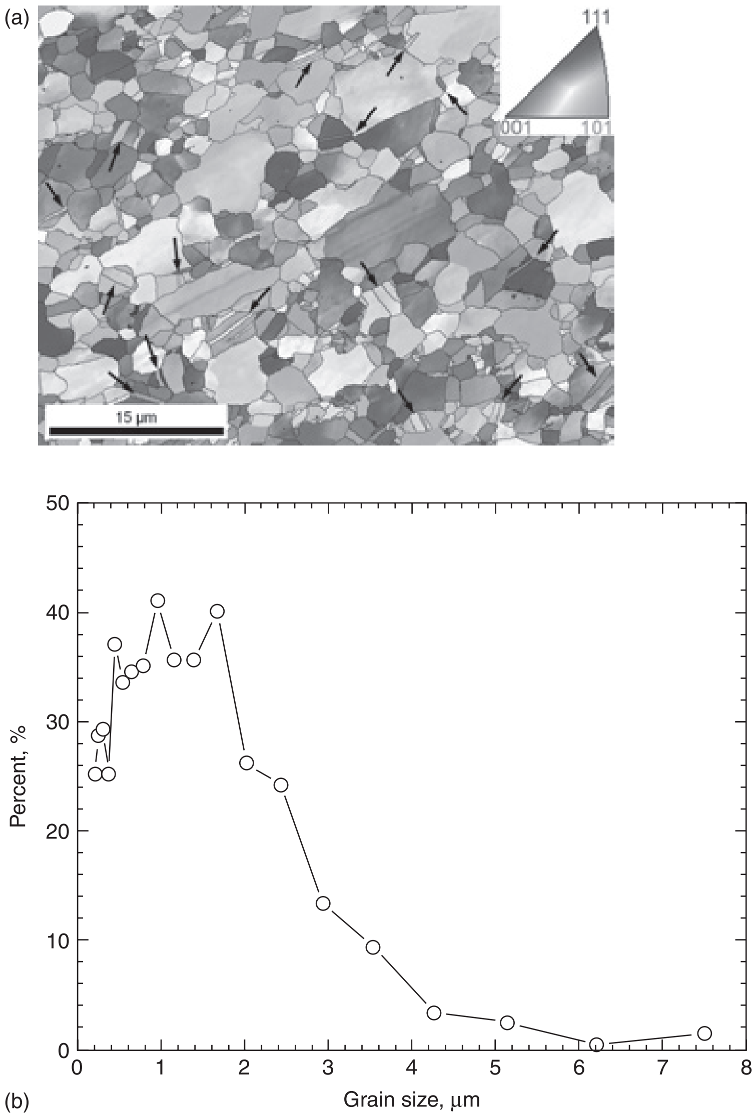

13.3 Electron backscattering diffraction (EBSD) crystal orientation mapping (a) and corresponding grain size distribution histogram (b) for multimodal Ni prepared by cryomilling and powder consolidation technique.[14] The inset indicates crystal orientations, and the black arrows point to twin boundaries.

strength and ductility in comparison with singular unimodal UFG or CG metallic materials.

Careful inspection of the literature indicates that investigations of multi-scale UFG metallic materials may be traced to their source in the late 1990s.

In 2000, Legros *et al.*[15] reported an attractive balance of some tensile ductility (2.1%) and yield strength (535 MPa) in a nanocrystalline Cu with a mean grain size of 26 nm and a multi-scale grain structure, while a nanocrystalline Ni, with a mean grain size of 28 nm and without the multi-scale grain structure (Fig. 13.4), experienced an entirely elastic deformation up to failure. The nanocrystalline Cu was prepared by inert-gas condensation[2] and subsequent warm compaction at 150°C as well as annealing at 150°C for 240 min. As a result, the nanocrystalline Cu specimen had significant volume fractions of UFG and few highly twinned 1–5 μm recrystallized CG grains. These UFG and CG grains were determined by the authors to be the microstructural reason for the higher ductility and lower flaw sensitivity compared with the nanocrystalline Ni.

In 2001, Tellkamp *et al.*[16] employed cryomilling and subsequent degassing, hot isostatic pressing and extrusion techniques to produce bulk commercial nanocrystalline 5083 Al alloys with both high yield strength (334 MPa) and good tensile ductility (8.4%), as shown in Fig. 13.5 (a). Their TEM observation revealed large grains next to an area with several small grains (Fig. 13.5 (b)), indicating a

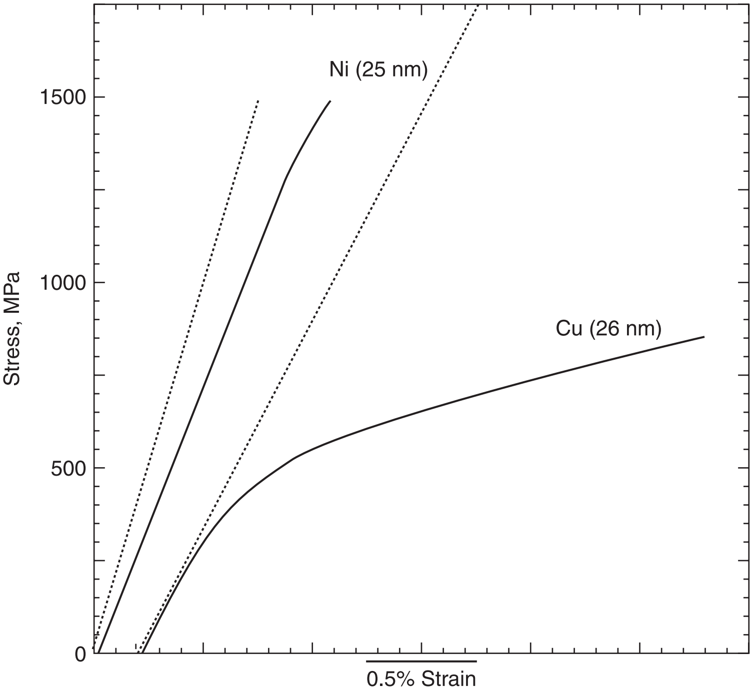

13.4 Tensile stress–strain curves of nanocrystalline Cu and Ni with mean grain sizes of 26 and 28 nm, respectively. The dotted lines indicate the linear elastic response.[15]

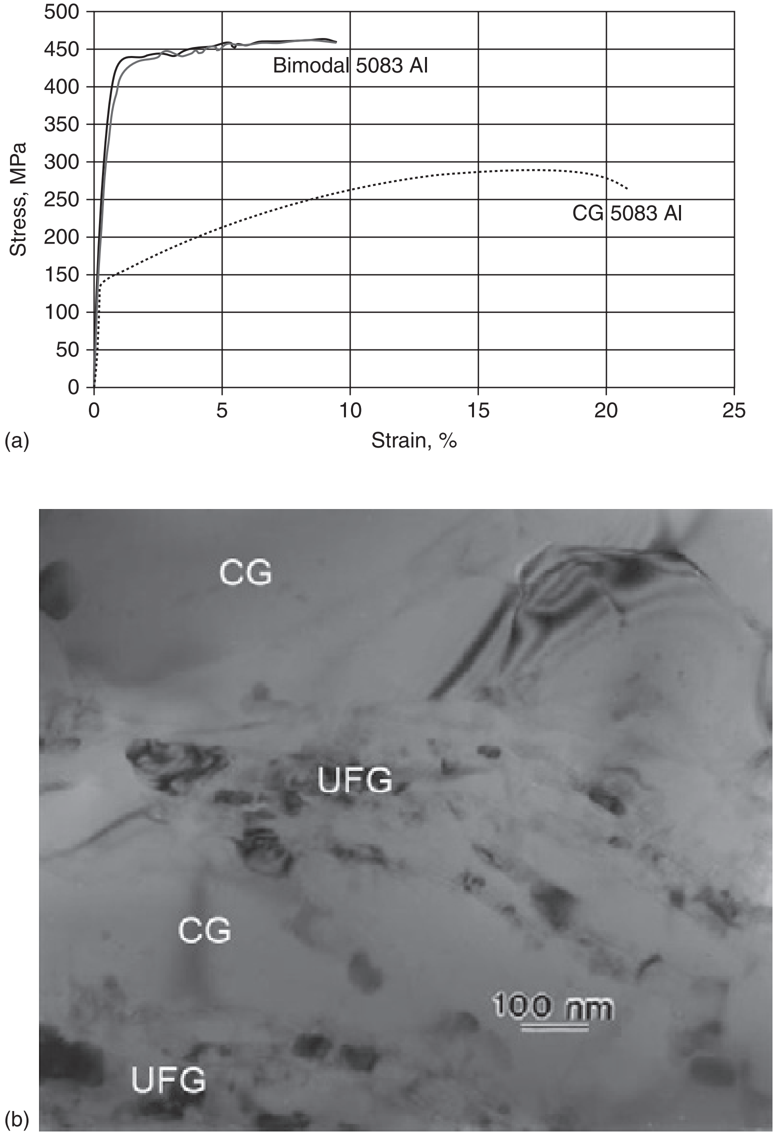

13.5 (a) Engineering tensile stress–strain curves of bimodal and coarse-grained 5083 Al alloys prepared by cryomilling and powder consolidation techniques. (b) Bright-field TEM image showing ultrafine grains (UFG) and coarse grains (CG).[16]

bimodal grain size distribution. A theory from the field of fracture mechanics was used to explain the good tensile ductility, as schematically shown in Fig. 13.6. A crack was initiated at an internal flaw and propagated rapidly through the UFG region with brittle precipitates at the GBs. The crack could be blunted by the

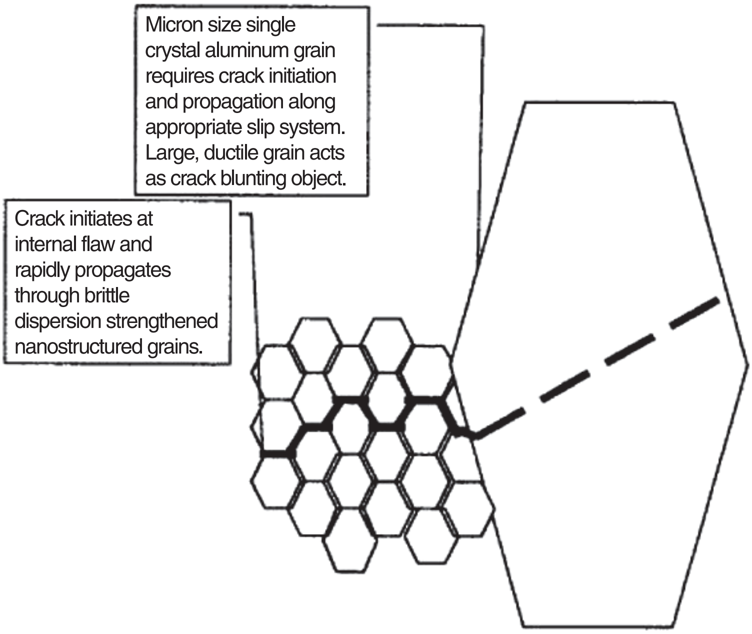

13.6 Proposed fracture theory for enhanced ductility of bimodal 5083 Al alloys. Cracks propagate quickly through the brittle UFG grains but are blunted by a large, ductile grain.[16]

large, ductile and single-crystal grains since it must propagate along the appropriate slip system of the large grains, and therefore, created ductility on a macroscopic level.

In 2002, Wang *et al.*[17] prepared a bimodal Cu with both high yield strength (320 MPa) and high tensile ductility (65% comparable to that of the CG Cu and 30% uniform elongation before necking instability occurs) by using a thermo-mechanical treatment (see Curve E in Fig. 13.7 (a)). The UFG Cu (Curve C) was prepared by cryorolling at liquid nitrogen temperature and had a vast majority of UFG grains. Annealing the as-rolled UFG Cu at 200°C for 3 min led to a bimodal grain structure with about 25% volume fraction of 1–3 μm CG grains embedded inside a UFG matrix with a mean grain size smaller than 300 nm. The CG grains were formed by abnormal grain growth (secondary recrystallization), and the UFG matrix was formed by a full primary recrystallization (Fig. 13.7 (b)).

The pioneering work of the above three groups of researchers has allowed the multi-scale grain size structure, as a generic and effective strategy, to be frequently employed to enhance the poor ductility of UFG metallic materials, such as Al[18,19] and Al alloys,[20–30] Cu.[31–35] Fe[36] and steels,[37–42] Ni,[14,43–45] and Ti.[46]

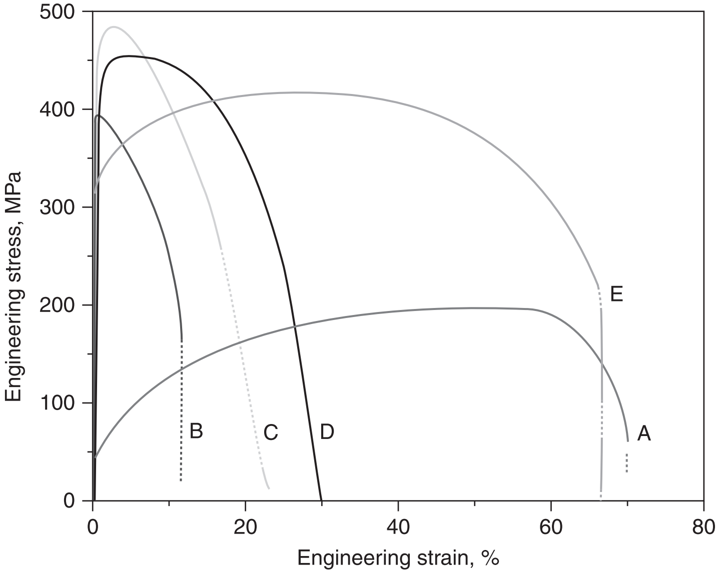

13.7 (a) Tensile stress–strain curves of coarse-grained Cu (curve A), ultrafine grained Cu (curves B–D) and bimodal Cu (curve E) prepared by thermo-mechanical technique.[17] (b) Bright-field TEM image of the bimodal Cu sample showing recrystallized coarse grains embedded in UFG matrix.

13.2 Mechanical properties of multi-scale metallic materials

Although a large amount of published work has qualitatively verified that the introduction of multi-scale grain structures can indeed improve the poor ductility of UFG metallic materials,[13–46] there are few systematic investigations to quantitatively characterize the relationship between the mechanical properties (strength and ductility) and the multi-scale grain structures.[13,17,22,25,47–55] These quantitative studies can be classified into two categories: experimental studies[13,17,22,25] and numerical studies.[47–55] The experimental approaches have inherent challenges in accurately controlling the multi-scale grain structures and their distributions. The numerical methods can more accurately yield carefully controlled grain size distributions; however, it is difficult to interpret the results and extrapolate the underlying mechanisms. The following section reviews the quantitative studies related to the mechanical properties of multi-scale metallic materials; first the experimental results and then the numerical results.

13.2.1 Experimental results

As discussed in the introduction, multi-scale grain structures can be introduced by either abnormal grain growth via annealing-induced secondary recrystallization of UFG metallic materials[13,17,22] or via the consolidation of mixtures of multi-scale size particles.[16,19,36] With the former technique, it is difficult to quantitatively control the multi-scale grain structures by controlling recrystallized nucleation sites and growth kinetics due to the highly unstable high-energy states of UFG microstructures.[17,56] The latter method allows for more accurate control of the multi-scale grain structures by simply controlling the mixing ratio of different-size particles. However, the processing artifacts, such as nano-pores and incomplete bonding that are sometimes introduced by the consolidation process, may obscure the intrinsic mechanical property–structure relationships.[20,21]

Inspection of the published literature related to the quantitative mechanical property–structure relationship of multi-scale metallic materials reveals a focus on bimodal metallic materials.[13,17,22,25] The following section first discusses quantitative experimental results of bimodal metallic materials and then addresses the topic of qualitative experimental results of multimodal metallic materials.[14,27,35,44]

Strength and ductility of bimodal metallic materials

The initial development and subsequent studies on multi-scale metallic materials discussed in the introduction inherently invoke a strategy of compromise: i.e. to achieve ductility, we must sacrifice strength. The question is: what is the relationship between the volume fraction of the components and the mechanical behavior? Can one predict the behavior of multi-scale metallic materials using simple weighted averages of the strength and ductility of UFG and CG components, i.e. following the rule-of-mixtures?[57] In the published literature, both positive (i.e. improved) and negative (i.e. diminished) deviations from the rule-of-mixtures have been reported. In the discussion that follows, we designate the positive case as a good combination of strength and ductility which stands out from the usual strength–ductility trade-off dilemma and has an extra gain in toughness; the negative case as a poor combination of strength and ductility; and the case complying with the rule-of-mixtures as the neutral or usual compromise between strength and ductility. In addition, there is one exception case reported for bimodal Ni, which was prepared by annealing an electrodeposited nanocrystalline Ni sample.[58] The bimodal Ni samples have both lower strength and ductility than the nanocrystalline Ni. It has been explained that the decrease in ductility of the bimodal Ni resulted from S and P impurity segregation at GBs, which caused GB de-cohesion and embrittlement.[58]

First, let us look at a good combination of strength and ductility that is better than the rule-of-mixtures (positive case). As described in the introduction, Wang *et al.*[17] reported that the introduction of 25% volume fraction of CGs into the UFG Cu matrix resulted in a 30% uniform elongation and a comparable elongation to failure (65%) with that of the CG Cu counterpart (70%), while the yield strength was still maintained at about 5–6 times higher than that of the CG Cu (Fig. 13.7). This, in fact, is an excellent compromise, because the simultaneous high strength and high ductility, especially the very large uniform elongation, results in a notable gain in toughness (the area under the stress–strain curve). To establish reproducibility, Wang *et al.* also annealed UFG Cu prepared by equal-channel angular pressing (ECAP)[59] and observed similar coexisting high strength and high ductility. Moreover, Wang *et al.* also reported further annealing beyond the bimodal structure shown in Fig. 13.7 (b) (i.e. 25% volume fraction of CGs) caused additional grain growth and larger uniform elongation, but with a large decrease in yield strength and no further gain in overall ductility. Wang's work suggests that a maximum combination of strength and ductility may exist when small amounts of CGs are embedded inside a UFG matrix, and that the combination (i.e. the toughness) decreases rapidly when the volume fraction of CGs are increased due to the rapid decrease in yield strength.

Similar results were reported by Jin *et al.*[22] with a 5754 Al alloy. The UFG Al alloy with duplex grain size distributions was prepared by asymmetric rolling and annealing. By treating the CGs with a size larger than 4 μm, and the UFGs with a size smaller than 4 μm, Jin *et al.* found both yield strength (YS) and ultimate tensile strength (UTS) increased linearly with increasing volume fraction of UFGs complying with the rule-of-mixtures, while the ductility of the 5754 Al alloy with duplex grain size distributions was comparable to that of the CG counterpart (~25%) when the CG content is 20–45%. Unlike in Wang's work, Jin *et al.* found that the ductility decreased with further increases of the CG content from 60 to 80%, and increased again to 25% when the CG content reached 100%.

Except for the above two papers, which reported a good combinations of strength and ductility in bimodal metallic materials, most related literature reports a poor combination of strength and ductility, which still complies with the strength–ductility trade-off dilemma.[13,19,25,32–34,36,43] Li *et al.*[13] performed a systematic study on the influence of CG content on the strength and ductility of bimodal Cu, and found that with increasing volume fraction of CGs, the strength decreased, and the ductility increased gradually to reach the value of the CG Cu

(42%), as shown in Fig. 13.8 (a). Yield strength and uniform elongation are inversely related, following a typical strength–ductility trade-off relationship (Fig. 13.8 (b)).

Here, the nanostructured (ns) Cu was prepared by DPD at liquid nitrogen temperature and consisted of about 33 vol.% nanoscale twin bundles embedded in 80 nm nanograins. Different volume fractions of CGs were introduced by static recrystallization (SRX). For instance, after annealing at 140°C for 10 min, the recrystallized CGs with a size ranging from 1 to 6 μm and a peak value of 2.2 μm were about 45% in volume, and the untransformed matrix consisted of the nanosized grains with a mean size of about 75 nm with nanoscale twin bundles (Fig. 13.2). After annealing at 200°C for 10 min, most of the sample was composed of SRX coarse grains with a mean grain size of 2.4 μm. The UFG Cu that was prepared by quasi-static compression (QSC) has a mean grain size of 290 nm. Annealing formed larger recrystallization grains (5 μm in mean) in UFG Cu. Most importantly, an obvious increment in the uniform elongation was achieved only when the volume fraction of SRX grains exceeded about 80% (Fig. 13.8 (c)). This volume fraction value of CGs is much larger than the value reported by Wang *et al.* where 30% uniform elongation was seen when CGs reached 25 vol.%. For

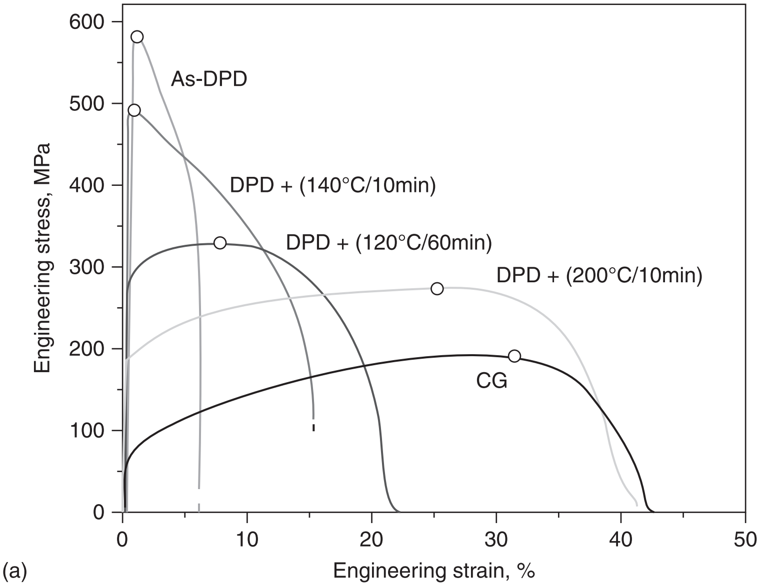

13.8 Tensile engineering stress–strain curves of bimodal Cu prepared by combination of DPD and annealing (as indicated) in comparison with the CG Cu. Uniform elongation is indicated for each sample by open circles.[13] (b) Plots of uniform elongation vs. yield strength for bimodal Cu samples prepared by annealing DPD,[13] QSC[13] and cryorolled[17] UFG Cu samples. (c) Variation of uniform elongation as a function of the volume fraction of SRX CG grains in various bimodal Cu samples.[13]

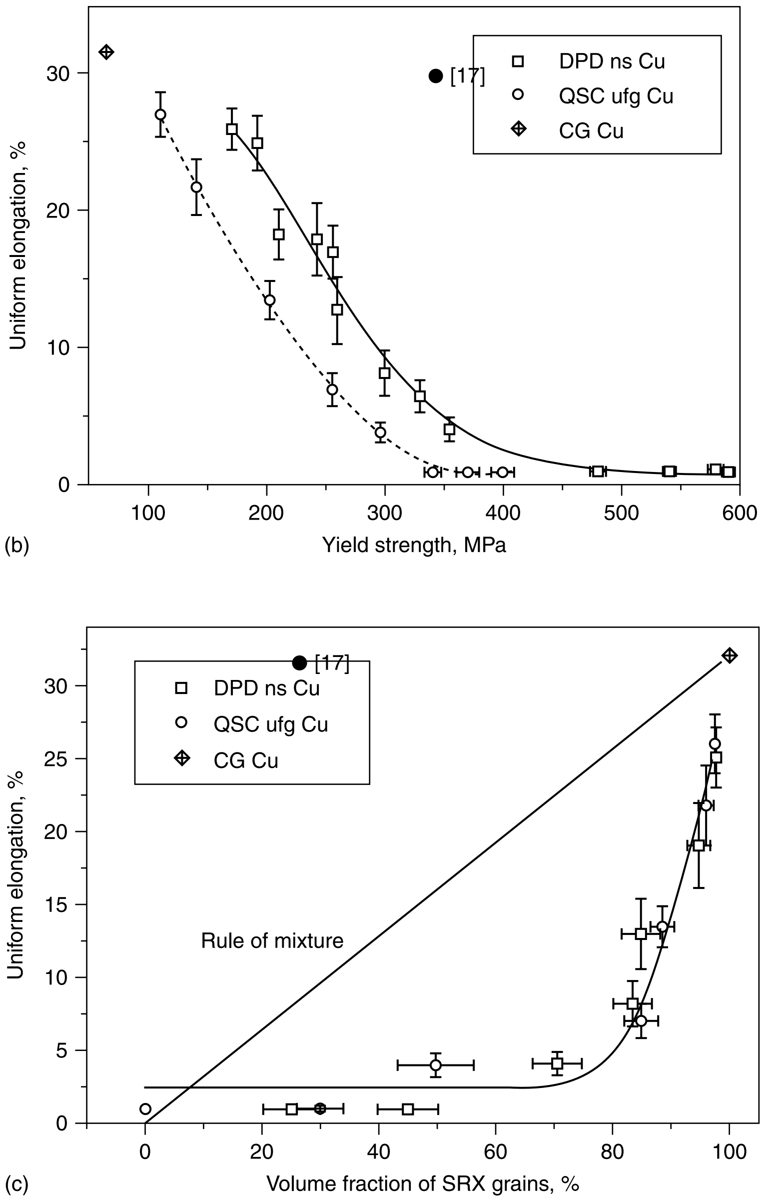

13.8 Continued.

comparison purposes, the data from Wang *et al.*[17] was also plotted in Fig. 13.8 (c). One can see that the data point of Wang *et al.* is far above the line of the rule-of-mixtures, suggesting positive deviation, while the data points from Li *et al.* are far below the rule-of-mixtures, suggesting a negative deviation.

Similar results were also reported by Han *et al.* with a bimodal 5083 Al-Mg alloy prepared by cryomilling and subsequent consolidation techniques.[25] An introduction of 30% volume fraction of CGs into UFG Al-Mg alloy matrix only extended the ductility to less than 3%, much smaller than the ductility of the CG Al-Mg counterpart (about 20%), suggesting a negative behavior. Here the bimodal Al-Mg alloys were produced by mechanically blending cryomilled UFG powders with 15 and 30% volume fraction of unmilled CG powders. The blended powders were then canned, consolidated by cold isostatic pressing, vacuum degassed and extruded at 550°C.[25] As a result, the CG regions with a mean grain size of about 1 μm extend along the extrusion direction and form discrete narrow bands surrounded by the continuous UFG matrix with grain sizes ranging from 100 to 400 nm. It should be noted that the consolidation methods might generate porosity, incomplete bonding, etc., artifacts that are known to be detrimental to tensile ductility. Nevertheless, the gradual decrease in strength and increase in ductility with annealing were also reported by many other groups in bimodal Cu prepared by cryorolling (Fig. 13.9 (a))[33] and ECAP (Fig. 13.9 (b)),[32,34] bimodal Ni by cryorolling (Fig. 13.9 (c)),[43] bimodal Fe by spark plasma sintering (SPS) of ball-milled powders,[36] and bimodal Al by ECAP consolidation with back pressure.[19] Although these papers did not report a quantitative relationship between strength/ductility and volume fraction of CGs, the strength–ductility combinations are either neutral or negative cases, rather than positive cases.

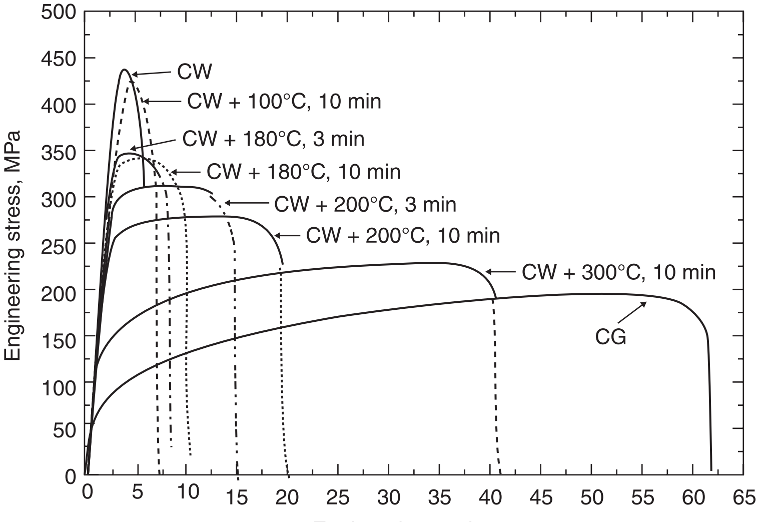

13.9 (a) Engineering stress–strain curves of bimodal Cu prepared by cryo-worked (CW) and annealing (as indicated).[33] (b) Engineering stress–strain curves of bimodal Cu prepared by ECAP and annealing/ cyclic deformation + ageing.[34] The ageing conditions are room temperature for 5 months. (c) Tensile stress–strain curves of bimodal Ni prepared by rolling at room temperature (RT) and liquid nitrogen (LN) and subsequent annealing (as indicated).[43]

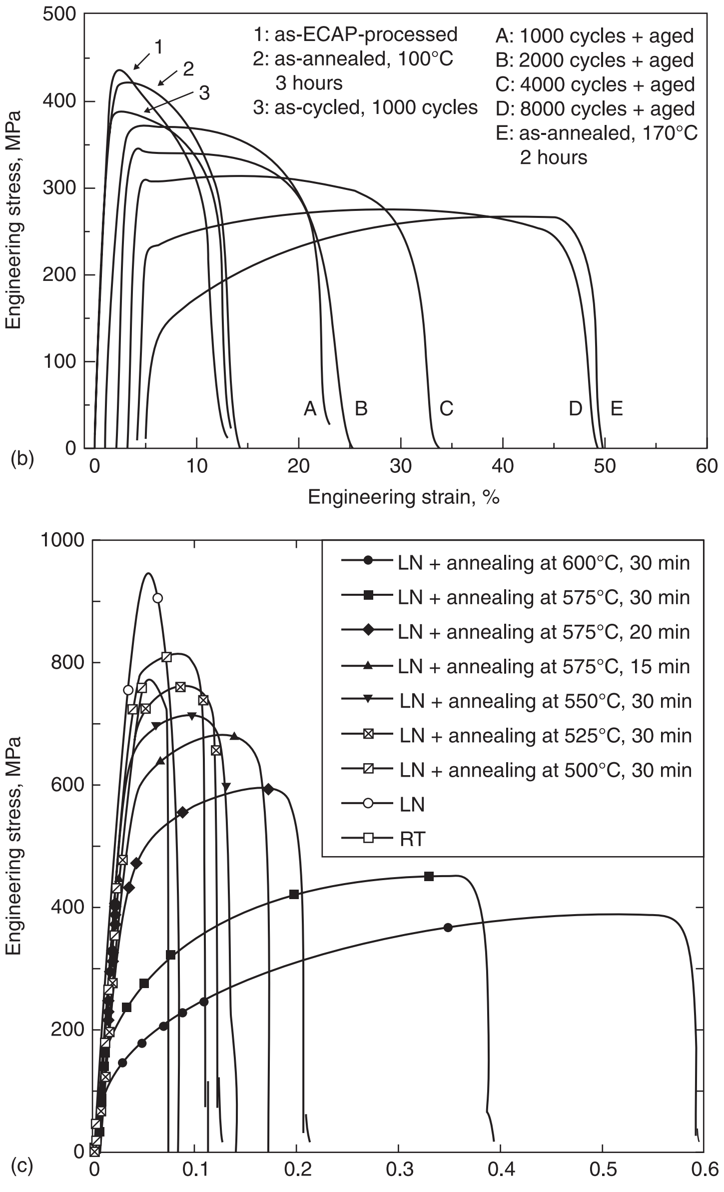

13.9 Continued.

In view of the fact that tensile ductility is sensitive to both extrinsic parameters (artifacts, temperature, strain rate) and intrinsic microstructures,[12] it is best to control one set of factors in order to reveal the quantitative relationship of strength/ductility and volume fraction of CGs in bimodal metallic materials. The data of bimodal metallic materials prepared by consolidation methods can be considered only when the processing artifacts are removed and ductility approaches an intrinsic value.[25] However, both good and poor strength–ductility combinations were observed in fully dense bimodal metallic materials that were artifact-free.[13,17,22] Possible reasons for the different results may be the differences in the detailed microstructures, such as the distribution of the UFG and CG grains, or grain size differences between the UFG matrix and CGs. As described in the introduction, multi-scale metallic materials have a wide grain size distribution, and the grain size distribution histogram, (i.e. volume fraction), is in fact not sufficient to describe the microstructures. For example, the connectivity of the large grains and small grains and their geometrical configurations are factors that need to be taken into consideration. They can be distributed homogeneously, as shown in Fig. 13.3 or heterogeneously, as shown in Fig. 13.2, which features a small-grain agglomerate and a large-grain agglomerate. The distribution of the grains may also have a significant influence on the mechanical properties. Therefore, systematic investigations are necessary to quantitatively reveal the mechanical properties and microstructure relationships of bimodal metallic materials.

Strength and ductility of multimodal metallic materials

The microstructure of bimodal metallic materials with double grain size distribution peaks is heterogeneous. The ductility of bimodal metallic materials is determined by the ductility of the UFG matrix, which has low strain hardening and plastic deformation capability. Therefore, cracks usually initiate in the UFG matrix or at the UFG and CG interface. In order to make the UFG matrix plastically deform continuously with the CG component and further increase the ductility, the concept of multimodal metallic materials with a continuous and wide grain size distribution is emerging as a variant of bimodal metallic materials.[14,27,35,44] In fact, many bimodal metallic materials in the literature are multimodal metallic materials since it is challenging to prepare bimodal metallic materials with two totally distinct grain size distributions.[13,15,22,25]

Research papers on multimodal metallic materials are very few. Shekhar *et al.*[35] reported a better combination of strength and ductility (yield strength 460 MPa and ductility 6%) in multimodal Cu than that in unimodal UFG Cu (yield strength 560 MPa and ductility 1.1%). The multimodal Cu was prepared by consolidating machined Cu chips and has a wide grain size distribution from UFG to several micrometers. Zhang *et al.* reported a larger ductility in multimodal 5083 Al (about 4%) than that in bimodal counterparts (3%).[27] The multimodal 5083 Al alloy was prepared by thermal consolidation of powders that were cryomilled for different times and had wide grain size distributions ranging from about 100 nm to 2.1 μm. The gain in ductility of multimodal 5083 Al alloy was obtained by sacrificing strength. Shen *et al.*[44] reported a better combination of strength and ductility in multimodal Ni than that in a bimodal Ni counterpart, which is correspondingly better than that in a unimodal Ni. The multimodal, bimodal and unimodal Ni were prepared by the electrodeposition method. The grain size in multimodal Ni ranged from about 10 nm to 160 nm.[44] Recently, Zhao *et al.*[14] prepared multimodal and bimodal Ni, with minimal processing artifacts, by quasi-isostatic Ceracon forging of cryomilled Ni powders, and found better strength–ductility combinations than the data reported in literature (Fig. 13.10 (b)). The multimodal Ni has a grain size distribution ranging from about 100 nm to 10 μm (Fig. 13.3), and the bimodal Ni from 100 nm to 30 μm (Fig. 13.10 (c)). Compared with the tensile data of the CG Ni (yield strength of 154 MPa and ductility of 48%), both multimodal and bimodal Ni have better strength and ductility combinations (471 MPa and 39%, 312 MPa and 49%, respectively), as shown in Fig. 13.10 (a).

In summary, available results suggest that a multimodal grain size distribution benefits ductility by sacrificing strength. Moreover, multimodal metallic materials exhibit combinations of strength and ductility that are superior to those of their unimodal counterparts. At present, the available published literature, however, does not unequivocally support the hypothesis that multimodal or bimodal metallic materials exhibit improved combinations of strength and ductility.

13.2.2 Numerical results

As discussed in the above section, although some progress has been documented, the challenge remains to synthesize samples that are defect-free and contain *a priori* design of multi-scale grain size distributions. Even the preparation of samples that contain a bimodal grain size distribution remains challenging because of mechanisms, such as grain growth, which are almost always operative. In an effort to circumvent these experimental challenges, while simultaneously providing insight into the operative mechanisms, numerical modeling is being widely applied to study multi-scale metallic materials. In the sections that follow, we review published numerical studies on the behavior of bimodal and multimodal metallic materials and compare and contrast the results.[47–55]

Strength and ductility of bimodal metallic materials

Inspection of the published literature shows that numerical studies on bimodal metallic materials predict behavior that is consistent (e.g. normal), and improved (e.g. positive), over the results obtained from a rule-of-mixtures rationalization. One example of a study that predicts behavior representing an improvement over the rule-of-mixtures was published by Sevillano *et al.*,[47] who used a one-dimensional cellular automaton model to simulate the elastic and plastic deformation of bimodal metallic materials. Examples of studies that predict a strength–ductility behavior that is consistent (e.g. normal behavior) with the rule-of-mixtures were reported by Raeisinia *et al.*,[55] who used a micromechanics polycrystalline model to simulate the monotonic plastic deformation of polycrystal with a bimodal grain size distribution, and by Joshi *et al.*[49] who applied a secant mean-field approach that approximated a bi-modal polycrystal as being composed of a coarse-grained phase embedded in an ultrafine-grained matrix. In the following sections the simulation results from these three studies are considered.

First we will address the case in which the strength–ductility relationship is predicted to exceed the trend anticipated from the rule-of-mixtures (e.g. the positive case). By using a one-dimensional cellular automaton model of gradient-dependent plasticity, Sevillano *et al.*[47] comparatively investigated the mechanical behavior of both unimodal and bimodal metallic materials. Figure 13.11 (a) shows several tensile true stress–strain curves calculated for a unimodal polycrystal with different mean grain sizes.

The tensile uniform elongation, indicated on each curve by open circles, increases first slowly and then rapidly with increasing the mean grain size or decreasing strength. Here b is the Burgers vector modulus, and the mean grain size of $<D> = 500b$ is approximately 130 nm for Cu, and $<D> = 10^5 b$ is about 25 µm. A narrow unimodal grain size distribution in the range of $<D> \pm 0.1<D>$ was assumed for UFG metallic materials. For larger grain sizes (i.e. $<D> = 25$ µm), the unimodal distribution was assumed to be wider ($<D> \pm 0.9<D>$). It is important

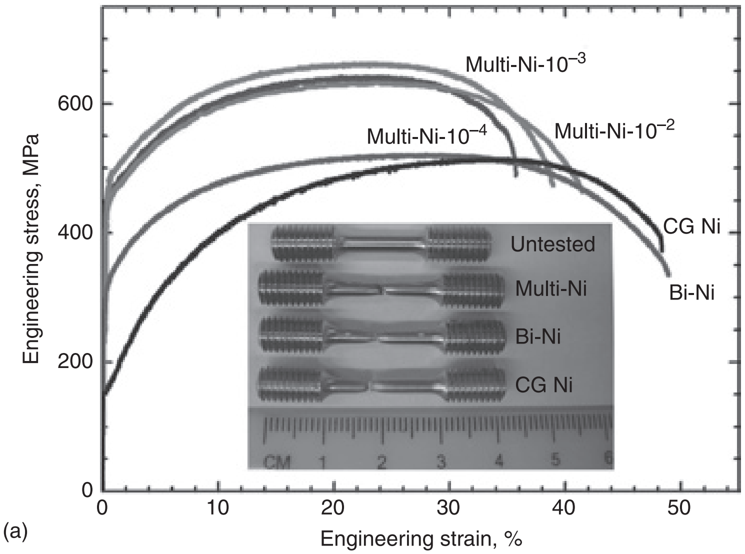

13.10 (a) Tensile engineering stress–strain curves of multimodal (Multi-Ni), bimodal (Bi-Ni) and CG Ni.[14] The Multi-Ni was tested at three strain rates: 10^{-2}, 10^{-3} and 10^{-4} s^{-1}, as indicated in the figure. The inset shows the picture of the fractured tensile specimens. (b) Yield strength vs. tensile ductility of Ni samples prepared by different techniques.[14] (c) EBSD crystal orientation mapping of bimodal Ni prepared by cryomilling and powder consolidation technique.[14] The inset indicates crystal orientations, and the black arrows point at twin boundaries.

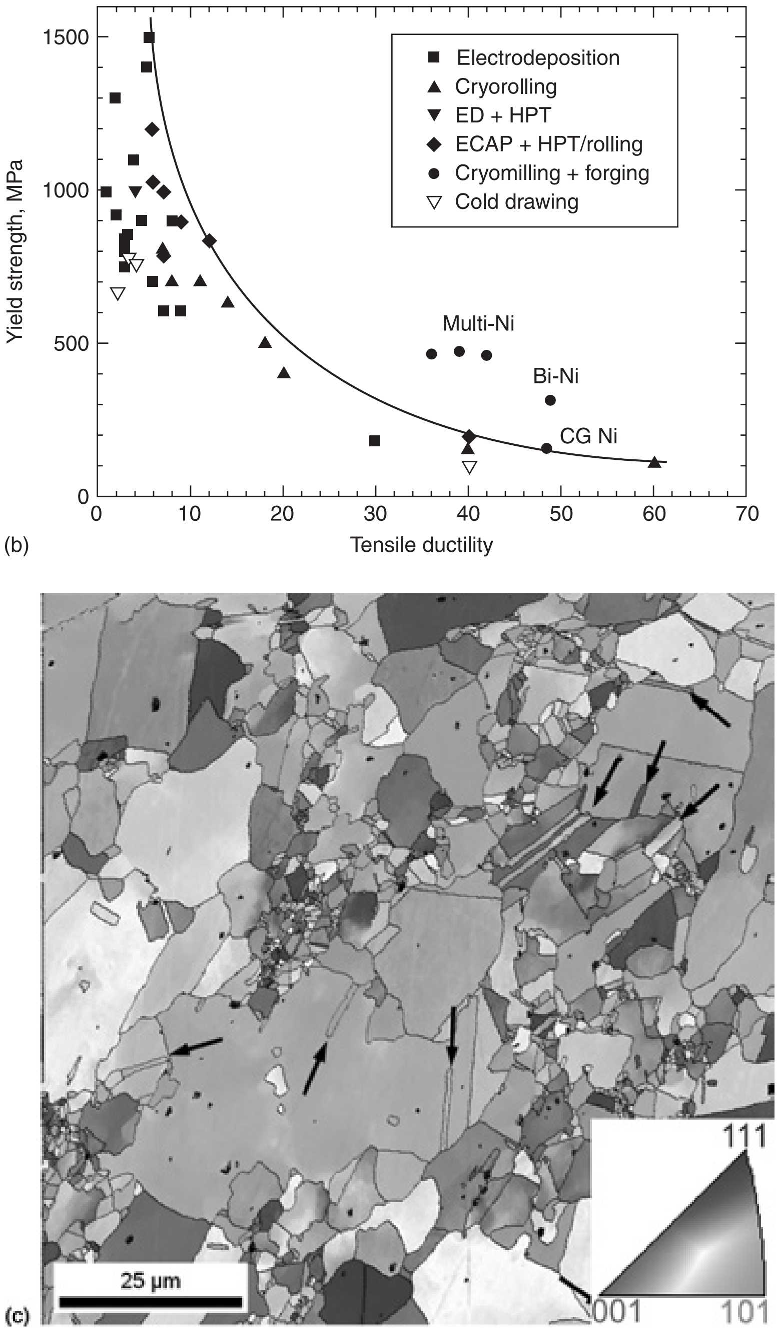

13.10 Continued.

to note the difference between unimodal grain size distribution and the multimodal grain size distribution. The latter has a much wider grain size distribution if one considers the range from UFG to CG region. For example, for the multimodal Ni as shown in Fig. 13.2, the average grain size <*D*> = 1 μm, and the grain size

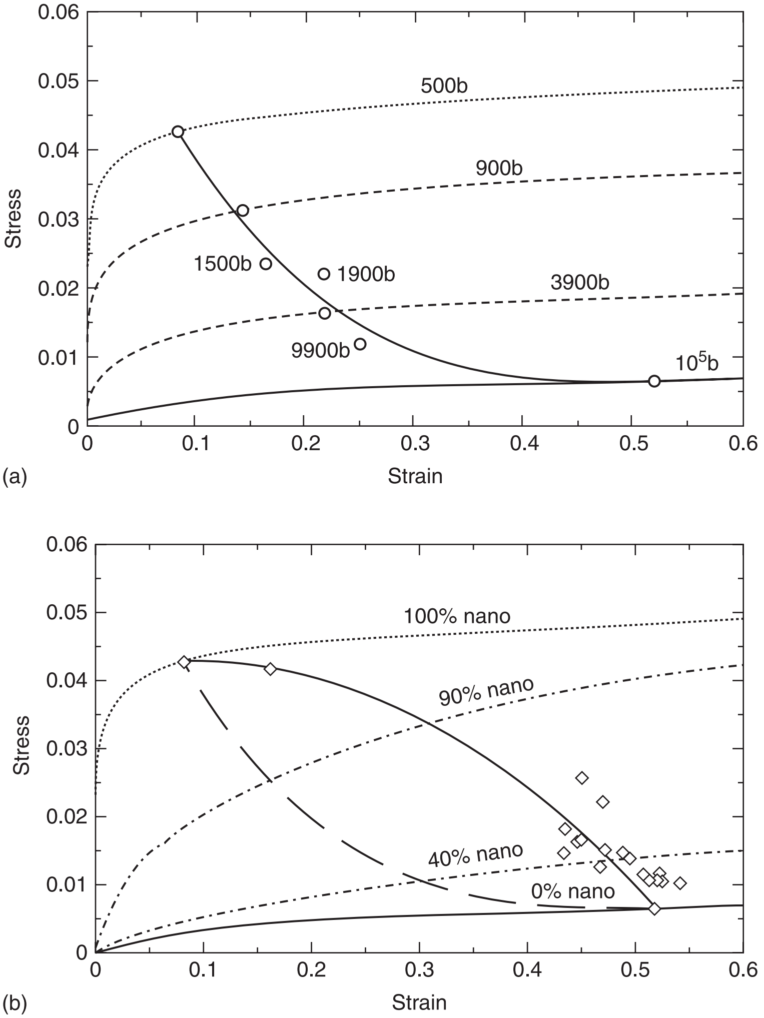

13.11 (a) Tensile true stress–strain curves calculated for polycrystals with unimodal grain size distributions of different mean grain sizes. Uniform elongations are indicated by open circles. (b) Tensile true stress–strain curves calculated for bimodal nanograin and coarse grain mixtures. Uniform elongations are indicated by open circles. Uniform elongations of unimodal polycrystals of similar strength (from a) fall on the dashed line. (c) Predicated uniform elongation of bimodal polycrystals vs. rule-of-mixtures approximation.[47]

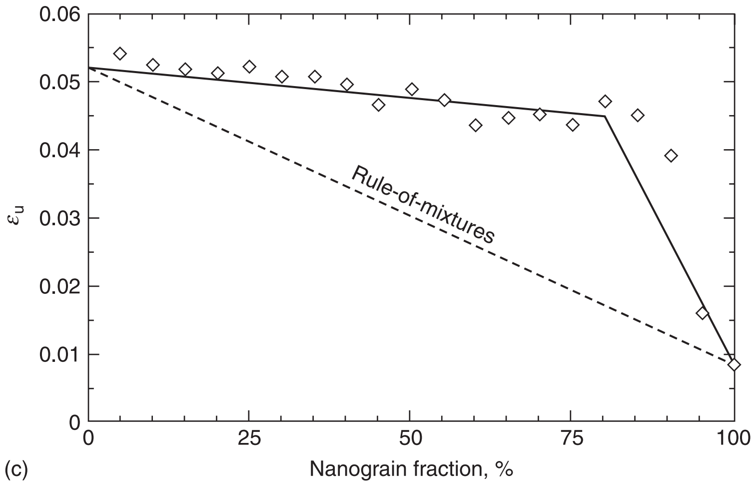

13.11 Continued.

distribution ranges from 0.1<*D*> to 10<*D*> where the large grain size is about two orders of magnitude larger than the small grain size. In contrast, the large grain size in a unimodal distribution is one order of magnitude of the small grain size, or both are at the same order of magnitude. Figure 13.11 (b) shows several tensile true stress–strain curves calculated for bimodal mixtures with different volume fractions of UFG matrix, as indicated in the figure. In this case the bimodal structures are randomly mixed with different (linear) fractions of the unimodal UFG structure (<*D*> = 500*b*, i.e. about 130 nm, uniform distribution in the range <*D*> ± 0.1<*D*>) and the unimodal CG structure (<*D*> = 10^5b, i.e. about 25 μm, uniform distribution between <*D*> ± 0.9<*D*>). The uniform elongation values for each curve are indicated by an open diamond. For comparison purposes, the ultimate tensile stress vs. the uniform elongation corresponding to the unimodal grain size distribution shown in Fig. 13.11 (a) is also shown in Fig. 13.11 (b) and is indicated by a dashed line. Different from that of the unimodal grain size distribution, the uniform elongation of the bimodal distribution increases first rapidly and then slowly with decreasing strength (i.e. volume fraction of UFG matrix). This results in a marked improvement in uniform elongation and the overall ductility of bimodal metallic materials relative to those corresponding to unimodal metallic materials possessing the same strength, i.e. a significant gain in toughness is attained by moving the curves towards upper-right corner. Sevillano *et al*. further argued that such a gain was obtained at the cost of a strength loss with respect to the unimodal UFG metallic materials, for instance, 10% of CGs in an UFG matrix produces only a 12% strength decrease relative to the 100% UFG metallic materials but increases the uniform elongation from less than 10% to near 40%. As a result, the ductility of bimodal polycrystal exceeds the prediction of the rule-of-mixtures, as shown in Fig. 13.11 (c). Moreover, the author further discussed that higher proportions of coarse grains induced important strength losses, resulting in yield stress or ultimate tensile stress values that fell below the rule-of-mixtures prediction. Sevillano and Aldazabal's numerical results discussed above are quite consistent with the experimental results reported by Wang *et al.*[17] and Jin *et al.*[22]

In contrast with the above numerical results in which the strength and ductility relationship deviated from the rule-of-mixtures in a positive way, Raeisinia *et al.*[55] and Joshi *et al.*[49] reported normal strength–ductility behavior for bimodal metallic materials, consistent with the predictions of the rule-of-mixtures. Figure 13.12 (a) shows the predicted stress–strain curves of a number of bimodal polycrystals constructed from different proportions of 200 nm ultrafine grains and 3 μm coarse grains. The 0% and the 100% indicate polycrystals with unimodal grain sizes of 200 nm and 3 μm, respectively. Here please note that, unlike Sevillano and Aldazabal's unimodal grain size distribution, which is in the range of <*D*> ± 0.1<*D*>, Raeisinia's unimodal metallic materials have the same grain sizes without any size distribution range, i.e. <*D*> ± 0.0<*D*>. All curves in Fig. 13.12 (a) were plotted to the end of uniform elongation as determined by Considère's criterion.[7] By incorporating 3 μm grains to the 200 nm grain matrix, the uniform elongation of the bimodal metallic materials is gradually restored at

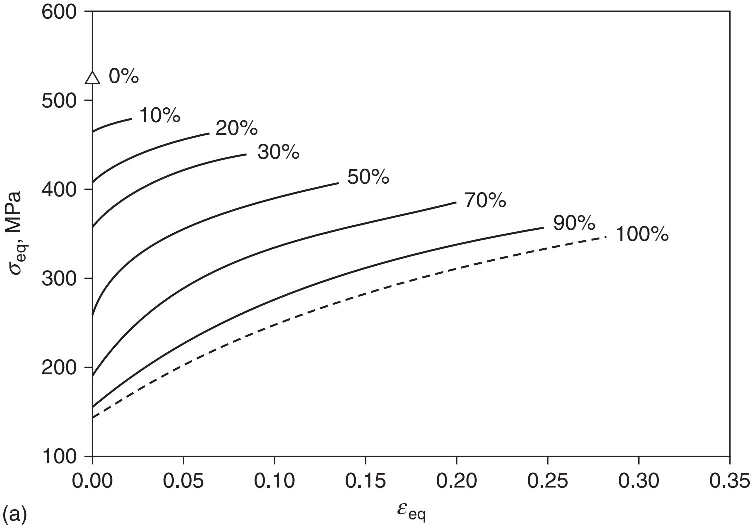

13.12 (a) Predicted von Mises equivalent stress–strain curves of bimodal polycrystals constructed from different proportions of 200 nm ultrafine grains and 3 μm coarse grains. The 0% and the 100% indicate polycrystals with unimodal grain sizes of 200 nm and 3 μm, respectively.[55] The variation of (b) ultimate tensile strength and (c) uniform elongation as a function of the volume fraction of coarse grain constituents (1 and 10 μm) for bimodal polycrystals with 200 nm UFG matrix.[55]

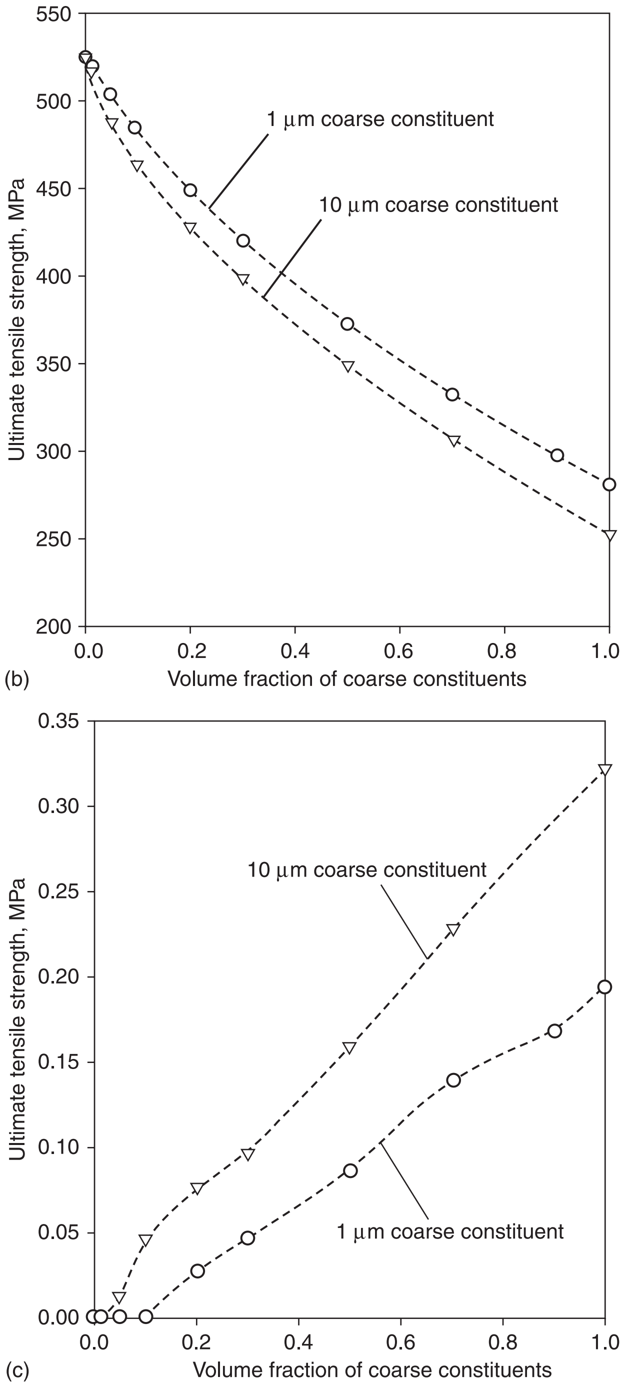

13.12 Continued.

the expense of the strength. Figure 13.12 (b) shows the evolutions of the ultimate tensile strength and the uniform elongation of the bimodal metallic materials having 200 nm UFG matrixes as a function of the volume fraction of their 1 or 10 μm coarse grain constituents. For the bimodal material with 1 μm coarse grains, the uniform elongation is zero when the volume fraction of CGs is smaller than 10%, and increases linearly with increasing the CG volume fraction more than 10%. When the CG constituent is a 10 μm grain, the uniform elongation has approximately linear relationship with the CG volume fraction, following the rule-of-mixtures prediction. Moreover, the ultimate tensile strength of the bimodal metallic materials decreased approximately linearly with increasing CG volume fraction (Fig. 13.12 (b)), also following the rule-of-mixtures. Raeisinia's numerical results indicate that it is possible to benefit from both the strengthening of the ultrafine grains and the high strain hardening capability (uniform elongation) of the coarse grains at intermediate volume fractions. Moreover, the larger coarse grain constituent has a marked positive influence on the uniform elongation relative to that of the smaller coarse grain constituent. Nevertheless, the strength–ductility combination follows the rule-of-mixtures without any additional gain in toughness as reported by Wang *et al.*,[17] Jin *et al.*[22] and Sevillano *et al.*[47] In addition, Joshi *et al.*[49] modeled the mechanical response of 5083 Al alloy with a bimodal grain size distribution by using the secant Mori–Tanaka (M–T) mean-field approach, and also reported that the ultimate tensile stress and uniform elongation follow the rule-of-mixtures prediction.

In summary, it is evident that there are significant differences in the predicted behavior of the strength–ductility relationship for bimodal metallic materials, which can be attributed in part to the various assumptions made in the development of the numerical models. What is perhaps more significant, however, is that the numerical results suggest that the strength–ductility relationship exhibits a marked dependence on the size, distribution and geometrical arrangement of the various constituent phases. Moreover, it is also evident that additional studies are required, which ultimately, with appropriate experimental verification, may be used to develop design principles that can be applied to multi-scale metallic materials, including those with a bimodal grain size distribution.

Strength and ductility of multimodal metallic materials

In this section, we review the numerical results related to the influence of the grain size distribution dispersion on the mechanical behavior of polycrystals, including those with multimodal and unimodal grain size distributions.

Numerical simulation results from different research groups indicate that the width of the log-normal grain size distribution has a significant influence on the yield stress, strain hardening and uniform elongation.[52,60–62] In an earlier study, Kurzydlowski[60] used a polycrystalline model based on the Hall–Petch relationship and the assumption that the portioning of plastic strain is proportional to the grain volume, to predict the influence of the dispersion of grain size distribution on the yield strength, and predicted that the slope of the Hall–Petch plot decreases with increasing degrees of dispersion. The prediction is consistent with a number of recent studies where numerical models that explicitly include a distribution of grain sizes and numerical approaches to partition stress and strain amongst the grains have been employed.[52,55,61,62] In the following section, we discuss some of the simulation results from Raeisinia *et al.*[55] who used a grain size dependent constitutive model within a viscoplastic self-consistent formalism to form a polycrystal with varying grain sizes and grain size distributions.

The generated log-normal grain size distributions with varying widths are shown in Fig. 13.13 in terms of: (a) number fraction and (b) volume fraction of grains. Here the grain size values, d, are normalized by the average grain size, µ. σ_0 is the standard deviation of the grain size distribution.[55] The dispersion of $\sigma_0/\mu \geq 0.8$ has a grain size range of 0.1µ–10µ, so it could be treated as multimodal grain size distribution.

Figure 13.14 shows the predicted yield strength as a function of square root of mean grain size for a variety of unimodal polycrystals with varying distribution widths. The Hall–Petch plot shows that increasing the width of the distribution results in a lowering of the yield strength, and the effect is stronger the smaller the mean grain size, resulting in a decrease in Hall–Petch slope.

Figure 13.15 depicts how the width of grain size distribution affects the stress (σ_{eq})–strain response (a and b) and the working hardening Θ behavior (c and d) of polycrystals with two different mean grain sizes of 700 nm (a and c) and 10 µm (b and d), respectively.

The von Mises equivalent stress–strain curves were plotted to the end of uniform elongation as calculated with Considère's criterion ($\Theta = \sigma_{eq}$). As the width of the distribution is increased, the uniform elongation of the polycrystal increases with a concomitant loss of some strength. At the same time, the strain hardening rate Θ increases, which can be used to rationalize the increased uniform elongation. Polycrystals with a 10 µm mean grain size behave similarly to their 700 nm counterparts, but the effect of the width of the distribution is much smaller. A similar grain size distribution dispersion effect on yield strength and uniform elongation was also reported by Malgin,[54] Morita *et al.*,[61] and Berbenni *et al.*[51,52] who used elastic–plastic formulations. In addition, by using a physical model, which includes Coble creep at fine grain sizes, Masumura *et al.*[63] have also concluded that the slope of the Hall–Petch is dependent on the width of the grain size distribution. Moreover, Phaniraj *et al.*[64] examined the influence of grain size distribution on the transition from grain boundary strengthening to grain boundary weakening in nanocrystalline metallic materials. This study reported that the transition becomes broader with an increase in the standard deviation of the grain size distribution.

In summary, with increasing grain size distribution dispersion (i.e. multimodal metallic materials), the uniform elongation and strain-hardening rate of a polycrystal increase by sacrificing strength. This, in fact, verified the above-mentioned experimental results reported for multimodal metallic materials.[14,27,35,44]

Comparison of bimodal and multimodal metallic materials

The numerical simulation results discussed above suggest that both bimodal and multimodal grain size distributions have a similar effect on the mechanical behavior of a polycrystal; i.e. an improvement in ductility is accompanied with a decrease in strength. Therefore, it is meaningful to accurately compare which distribution (i.e. bimodal or multimodal) has a stronger influence. To that effect, in a recent study, Raeisinia *et al.*[55] compared different bimodal, multimodal and unimodal polycrystals with one another, as plotted in Fig. 13.16 in terms of the ultimate tensile strength versus the uniform elongation.

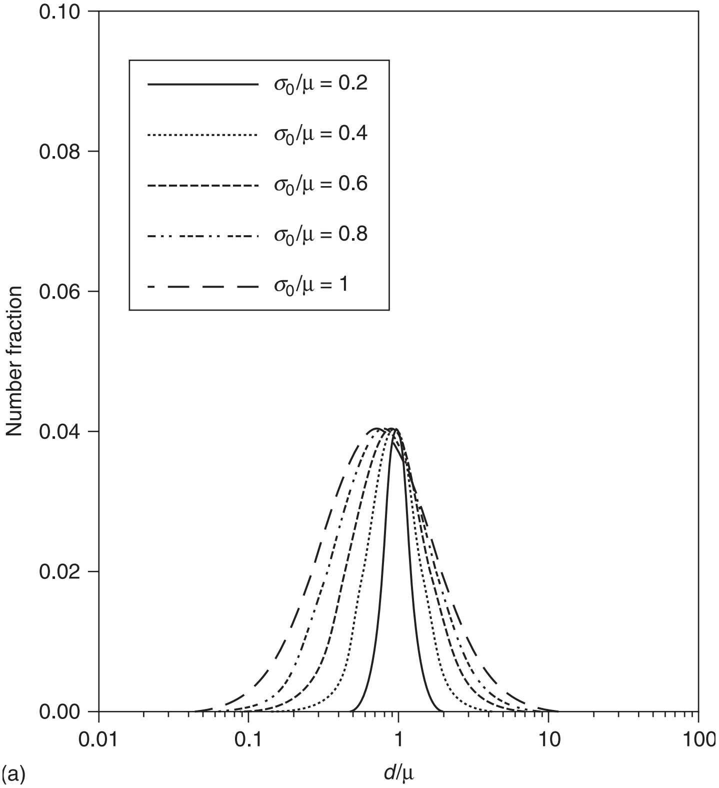

13.13 Generated log-normal grains size distributions with varying widths shown in terms of (a) number fraction and (b) volume fraction of grains. The grain size values, d, are normalized by the average grain size, μ. σ_0 is the standard deviation of the grain size distribution.[55]

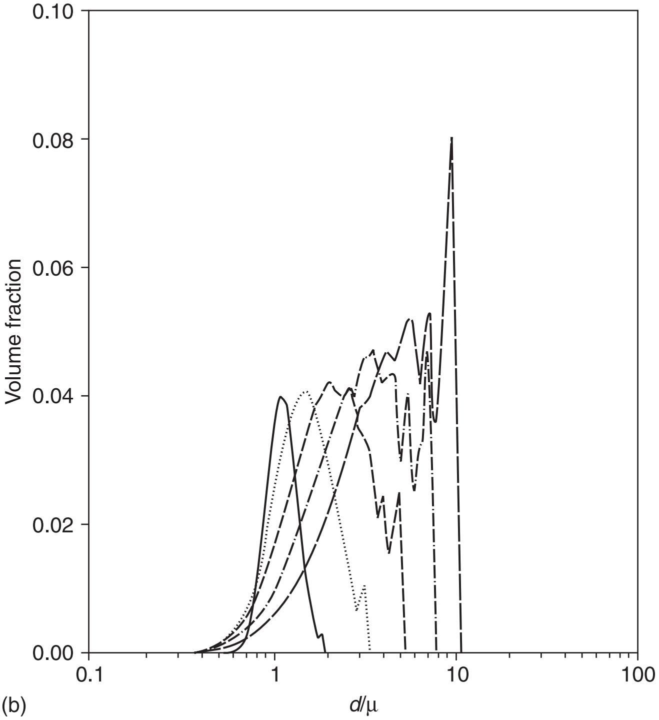

13.13 Continued.

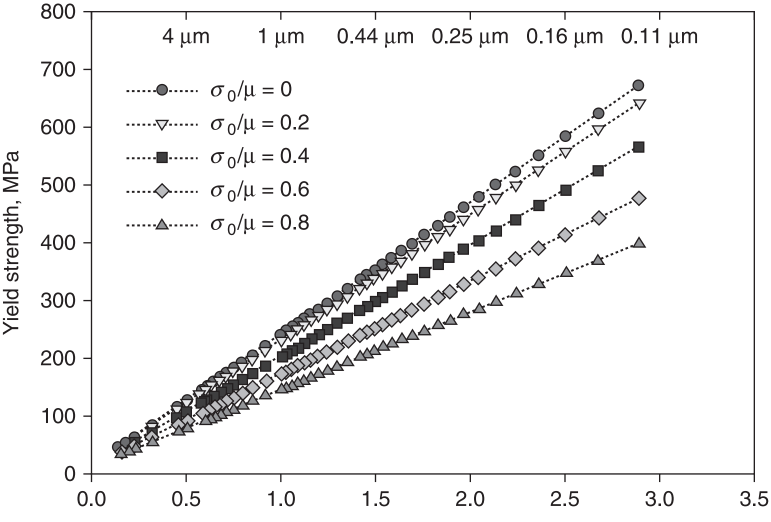

13.14 Predicted yield strength as a function of square root of mean grain size for a variety of unimodal polycrystals with varying distribution widths.

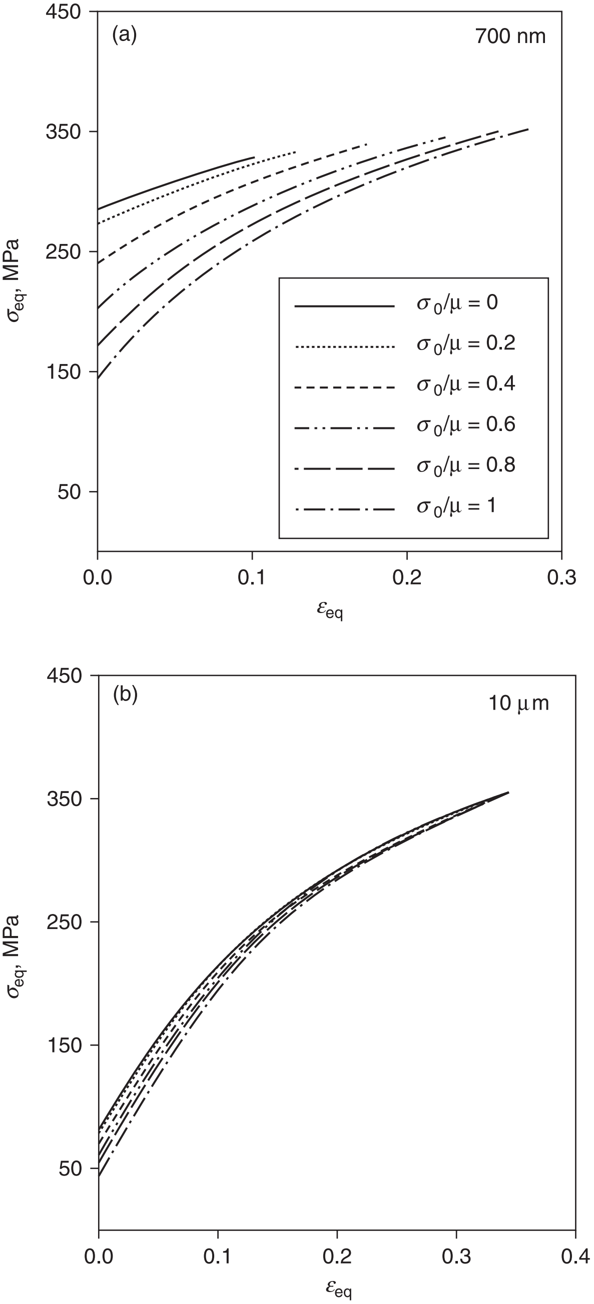

13.15 Calculated von Mises equivalent stress–strain curves and strain hardening Θ plots of polycrystals with 700 nm (a, c) and 10 µm (b, d) mean grain size and varying widths of distributions. In (c) and (d), the $\Theta = \sigma_{eq}$ line correspond to the Considère criterion.[55]

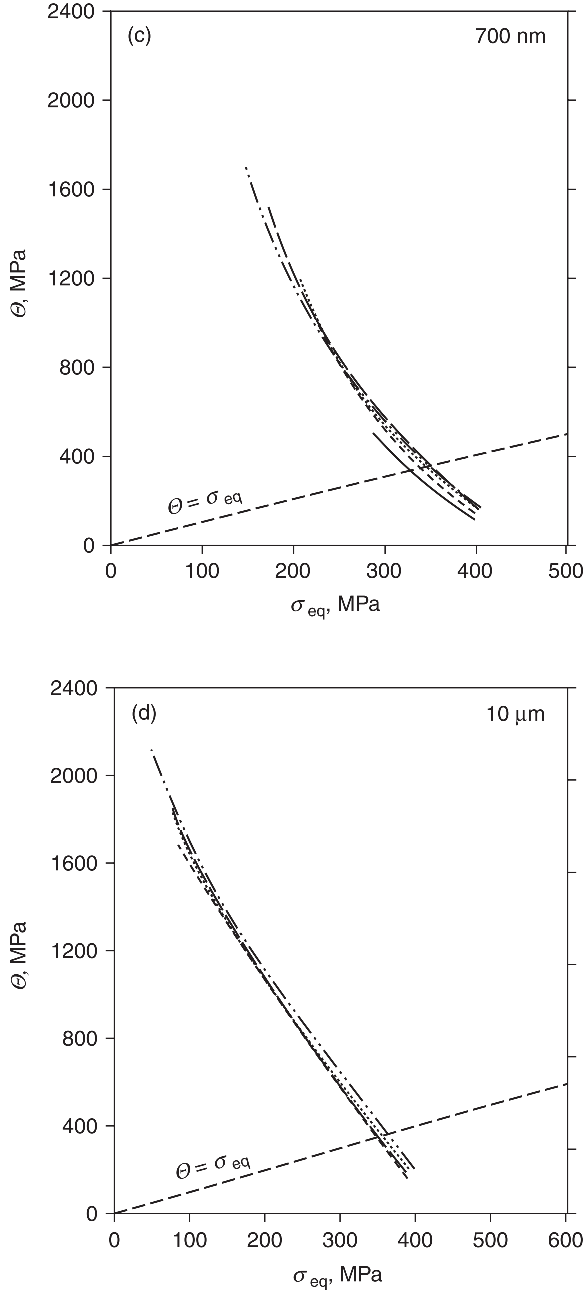

13.15 Continued.

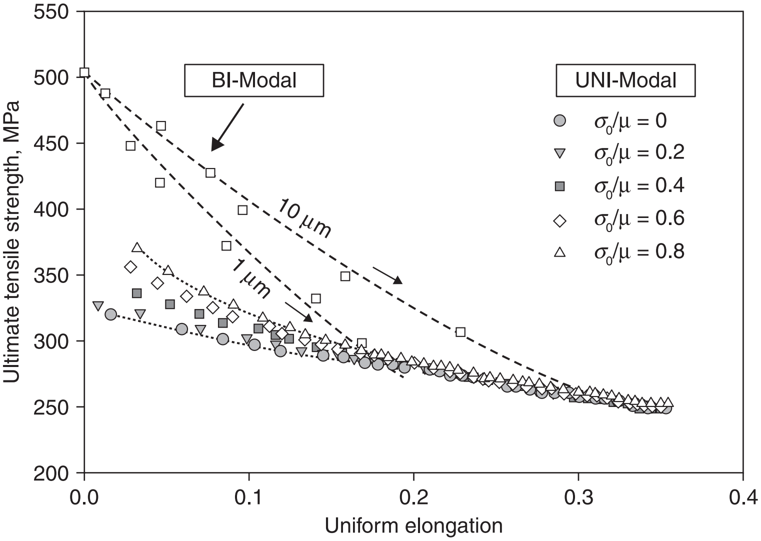

13.16 Tensile strength vs. uniform elongation predicted for bimodal, unimodal and multimodal ($\sigma_0/\mu = 0.8$) metallic materials. The bimodal metallic materials have 200 nm UFG matrix and either 1 or 10 μm CG constituents. The arrows on the dashed lines show direction of increase in the volume fraction of CG constituents of bimodal metallic materials. For unimodal and multimodal metallic materials, the mean grain size μ ranges from 100 nm to 50 μm for each distribution width.[55]

The multimodal/unimodal polycrystals are of different average grain sizes (μ values ranging from 100 nm to 50 μm) and grain size distributions (σ_0/μ ratio varying from 0 to 0.8), while bimodal polycrystals all have 200 nm UFG matrix and varying volume fractions of either 1 or 10 μm grains as their coarse constituents. Arrows on the dashed lines show the direction of increase in the volume fraction of the coarse constituents of the bimodal polycrystals. In the case of the unimodal polycrystals, uniform elongation exhibits a dispersion at smaller values which results from the improvement observed in uniform elongation of unimodal UFG polycrystals when the width of their size distribution is increased (as shown in Fig. 13.14). With increasing mean grain size, the dispersion in uniform elongation caused by grain size distribution dispersion gradually diminishes. As compared with unimodal and multimodal polycrystals, the bimodal polycrystals populate new regions of the ultimate tensile strength-uniform elongation space by shifting the strength-uniform elongation envelope defined by unimodal and multimodal polycrystals favorably towards higher strength and elongation. This result indicates that the bimodal grain size distribution has a better strength–ductility combination than that of the multimodal distribution. Moreover, a larger coarse grain constituent (such as 10 μm) shows a better strength–ductility combination when compared to that of a smaller coarse grain constituent (1 μm). The values for bimodal polycrystals represent upper limit

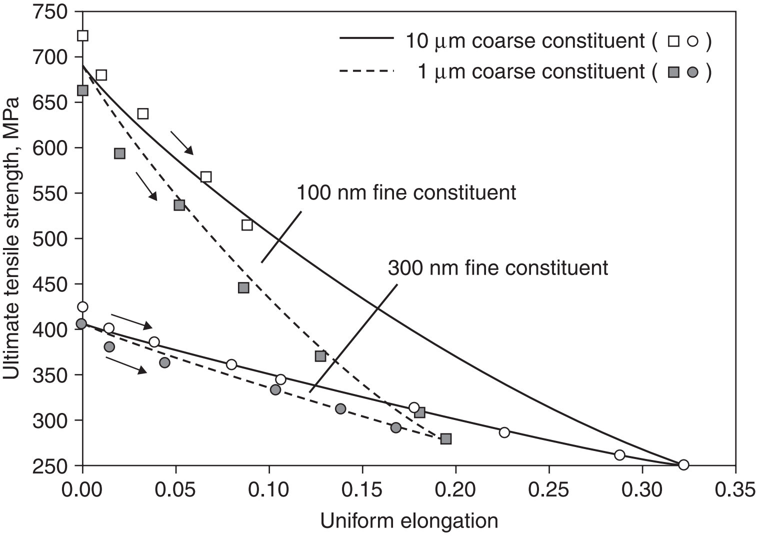

13.17 Plot of ultimate tensile strength vs. uniform elongation for bimodal metallic materials having 100 and 300 nm UFG matrix and 1 and 10 μm CG constituents.[55] The arrows on the solid and dashed lines show direction of increase in the volume fraction of CG constituents.

estimates, because only bimodal structures with same-size ultrafine and same-size coarse grains were considered and as the ultrafine and coarse grains start to develop size distributions, the values of bimodal polycrystals will tend towards the unimodal values.

Raeisinia *et al.*[55] further examined the effect of varying the size of the UFG constituent on the strength-uniform elongation combination, as shown in Fig. 13.17. The ultrafine grains are designated as 100 and 300 nm, respectively. Aside from shifting either of the lines towards higher strength and uniform elongation, a decrease in the size of the UFG constituent also tends to amplify the difference between 1 and 10 μm. This means that as the behavior of the ultrafine grains approaches that of the coarse grains, or in other words the strength effect of the ultrafine grains vanishes, there is less improvement to be obtained in the strength–ductility response.

In summary, the results described above suggest that a bimodal grain size distribution has an advantage in improving the combination of strength and ductility relative to that attainable with a multimodal grain size distribution.

13.3 Deformation and fracture mechanisms of multi-scale metallic materials

The mechanical properties of multi-scale metallic materials (such as ductility) depend on the relevant deformation and fracture mechanisms that are activated during loading. An inspection of the published literature reveals that investigations on the deformation and fracture mechanisms of multi-scale metallic materials deal principally with microstructures that contain a bimodal grain size distribution, for both experimental studies as well as numerical simulations. In the sections that follow, we first introduce the deformation and fracture mechanisms that are active in metallic materials with a unimodal grain size distribution, and then discuss the mechanisms that relate to bimodal metallic materials.

13.3.1 Deformation and fracture mechanisms of unimodal metallic materials

Figure 13.18 schematically shows the deformation mechanisms of a face-centered cubic polycrystal with medium- and high-stacking fault energy as a function of grain size.

When the grain size falls in the nanometer regime (say <10 nm), a transition of the dominant deformation mechanisms from the usual dislocation-mediated

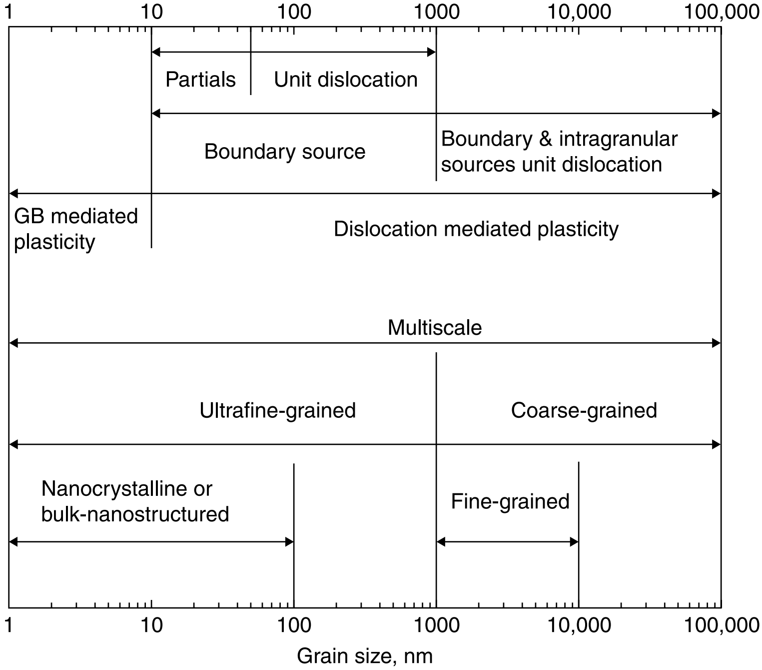

13.18 Schematic representation of deformation mechanisms of a face-centered cubic polycrystal with medium and high stacking fault energy versus gain size.

plasticity to grain boundary-mediated processes takes place which corresponds to a transition in the slope of Hall–Petch relationship.[4,65–70] The grain boundary-mediated processes include grain boundary sliding, migration and grain rotation.[71–84] The macroscopic plastic deformation capability of nanocrystalline metallic materials with grain boundary-mediated processes is usually very limited under conventional deformation conditions,[73] unless under some specific conditions such as dynamic loading,[84] miniature sample geometries,[85–87] or deformed at elevated temperature[88–90] which promote the activation of boundary process. In contrast, when the grain size falls in the micrometer regime (>1 μm), intragranular dislocation activity plays a dominant role in plastic deformation.[1] Micrometer-sized grains generally provide sufficient space for dislocation activity, such as nucleation, dislocation tangling, cutting and propagation and as a consequence, the associated strain hardening results in a high tensile ductility.

When the grain size is smaller than 1 μm and larger than about 10 nm, grain boundaries act as both dislocation sources and sinks, and they lead to the absorption of dislocations by grain boundaries as soon as the dislocations are emitted from the opposite boundaries.[4] Since very few dislocations can accumulate within ultrafine grains, the resultant strain hardening is very low, resulting in limited tensile ductility. In related studies, it was experimentally shown that, under the right conditions, such as at a very low strain rate of 10^{-5} s^{-1} or elevated temperatures, grain boundary sliding could be activated in UFG metallic materials with a mean grain size larger than 100 nm.[78,88–90,91,92] However, under normal deformation conditions, grain boundary sliding is limited and hence does not contribute to the poor ductility of UFG metallic materials with a unimodal grain size distribution. When the grain size is smaller than about 50 nm, deformation twinning has been frequently reported even in metallic materials with medium to high stacking fault energies such as Cu and Ni, and this has led to the suggestion that twinning is a major plastic deformation mechanism in UFG metallic materials.[93–96] Systematic high-resolution TEM studies revealed that the deformation twinning in UFG metallic materials was formed by the emission of Shockley partial dislocations from grain boundaries.[67,73] A more recent study indicates that further decreasing the grain size of UFG metallic materials actually impedes twinning (i.e. inverse grain size effect), which was explained using generalized planar fault energies and grain size effects on the emission of partial dislocations.[97]

In reference to fracture mechanisms, both ductile and brittle fracture processes are reported to occur in nanocrystalline metallic materials, and there are several examples showing ductile fracture in metallic materials with an average grain size in range from 20 to 100 nm.[4,98–101] Most of these experiments provide support to the suggestion that in nanocrystalline metallic materials the nucleation of cracks occurs at grain boundaries and triple junctions. For example, Kumar *et al.* examined deformation mechanisms and damage evolution in nanocrystalline Ni prepared by electrodeposition.[98,99] It was reported that dislocation emission at grain boundaries, together with intragranular slip and unaccommodated grain boundary sliding facilitate the nucleation of voids at boundaries and triple junctions. When exposed to extensive local plasticity, these voids, as well as those that may have existed prior to deformation, can behave as nucleation sites for dimples leading to fracture that do not occur preferentially along grain boundaries. Moreover, Ovid'ko *et al.*[102] reported that plastic deformation in a nanocrystalline solid is strongly influenced by the presence of interfaces. In particular, grain boundaries hinder intragranular slip activated by lattice dislocations. These hindering mechanisms are related to the formation of disclination dipoles where nanocrack nucleation occurs. In the case of UFG metallic materials with a mean grain size larger than 100 nm, numerous available experimental studies reveal that they fracture in a ductile way.[4,103]

13.3.2 Deformation and fracture mechanisms of bimodal metallic materials

Available published studies on the deformation and fracture mechanisms that are active in bimodal metallic materials provide useful fundamental insight into their strength and ductility behavior. Unfortunately, however, such studies are limited, and often only preliminary results are available. In the sections that follow, we introduce deformation and fracture mechanisms in bimodal metallic materials for both tension and compression conditions.

Tension

To provide insight into the mechanisms responsible for the excellent combination of strength and ductility reported for bimodal Cu, Wang *et al.* applied finite element modeling in combination with post-mortem TEM analysis.[17] They reported that during deformation, the CGs that are embedded in the heterogeneous microstructure experience multi-axial stress state conditions, consisting of a complex strain field with a triaxial strain component, and very large strain gradients (Fig. 13.19).

Under these stress state conditions, strain–gradient plasticity theory[104] suggests that an excessively large number of geometrically necessary dislocations is required to accommodate the large strain gradients, thereby resulting in significant strain hardening and large uniform elongation. Moreover, deformation twinning was observed after straining for 6% inside most of all of the CGs (Fig. 13.20 (a)).

High resolution TEM, as shown in Fig. 13.20 (a) lower-right corner, shows twin boundaries located preferentially near the extrusions of the surrounding UFGs into the softer CGs, suggesting that the constrained CGs plastically deform at high stresses, which results in twinning initiation presumably due to stress

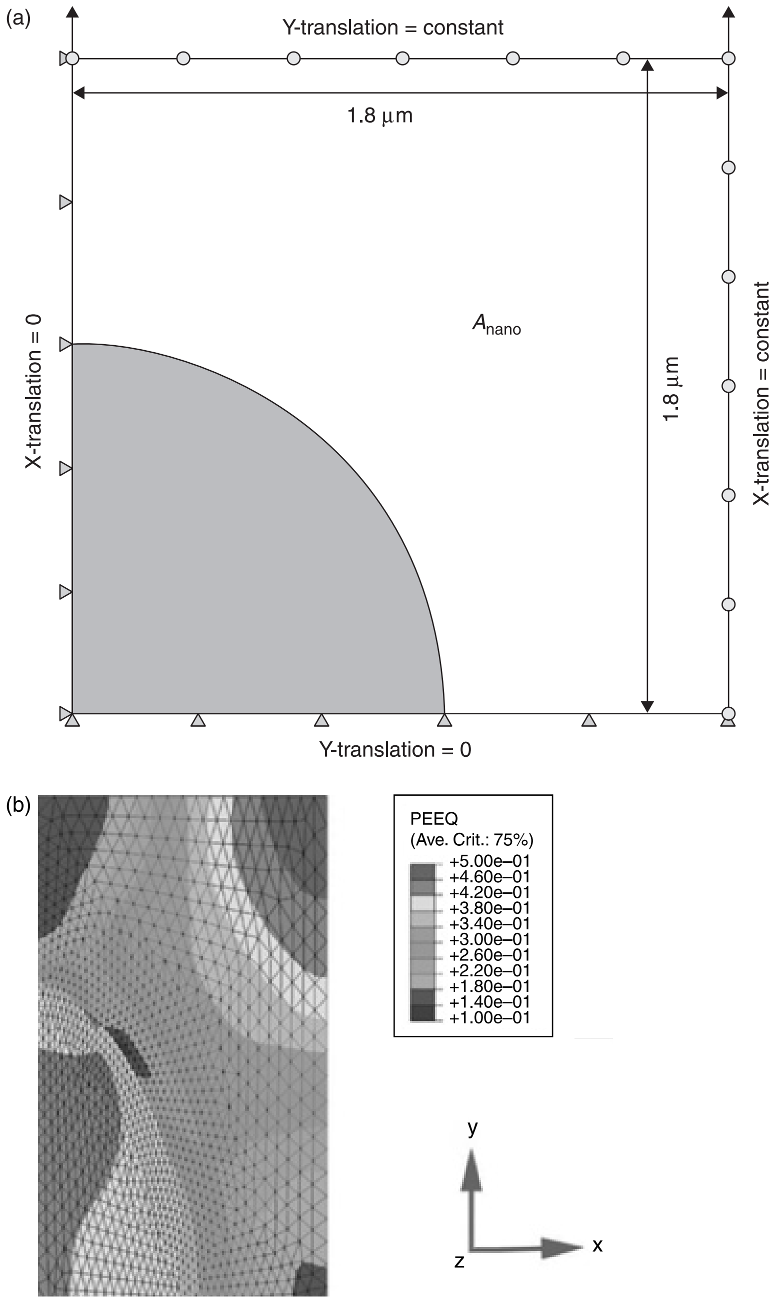

13.19 The finite element modeling of the bimodal Cu. (a) Micrometer-sized grains (A_L) embedded inside UFG matrix (A_{nano}). (b) The large strain gradient observed across CG and UFG grains.[17]

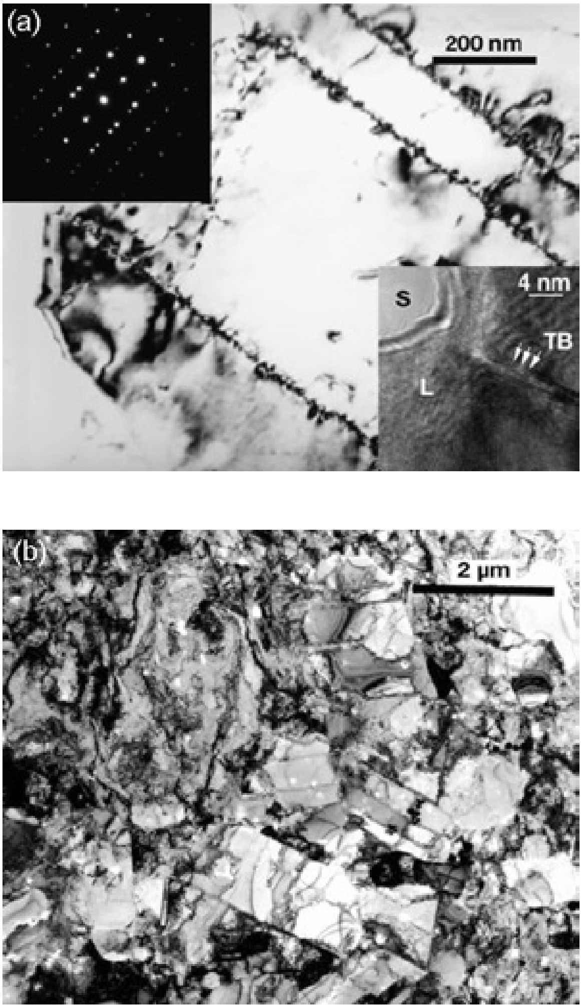

13.20 (a) Transmission electron microscopy image of the CG in bimodal Cu sample after 6% plastic strain.[17] The upper left inset shows the twin relationship, and the lower right inset shows high-resolution TEM image of the interface of CG (L) and UFG (S) matrix.
(b) Transmission electron microscopy image of bimodal Cu after 30% uniform strain.[17]

concentration. Twin boundaries can be considered to be a special type of high angle boundary, and hence are known to effectively increase strain hardening via dislocation accumulation.

In summary, the deformation of the bimodal Cu can be described as follows. During loading, the CGs accommodate the strains preferentially. By the time the overall uniform elongation has attained a value of approximately 30%, the large-grain CGs have accumulated large numbers of twin boundaries, dislocations and subgrain boundaries, such that their microstructure is refined to a level similar to that of the UFG matrix (Fig. 13.20 (b)). Beyond this point, the post-necking deformation is similar with that of the unimodal UFG metallic materials. Therefore, these results suggest that the presence of a heterogeneous microstructure is required to attain good combination of both high strength and high ductility.

Recently, Lee *et al.*[30] investigated deformation and fracture mechanisms of a bimodal Al-Mg alloy containing 30% volume fraction of CGs prepared by cryomilling and subsequent powder consolidation techniques. The microstructures of the bimodal Al-Mg alloy are shown in Fig. 13.11. Room temperature tensile studies show a good balance between strength and ductility for the bimodal sample in comparison with the results for the unimodal UFG and CG counterpart metallic materials (Fig. 13.21). As shown in the inset fracture end cross-section in Fig. 13.21, the unimodal UFG sample exhibits a fully flat fracture and involves a brittle transgranular shear type separation, caused by incomplete bonding and possibly by the presence of some processing artifacts due to consolidation processing.

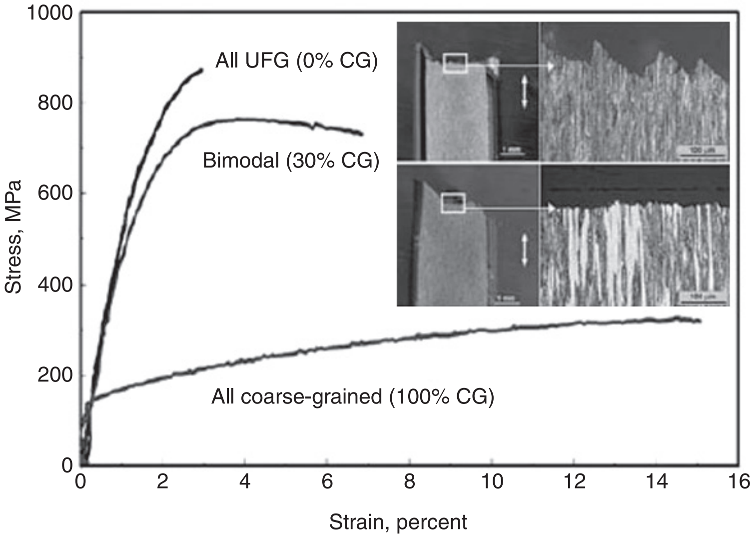

13.21 Tensile stress–strain curves of bimodal Al-Mg alloy with 30% volume fraction of CGs compared with unimodal UFG and CG counterparts.[30] The insets are cross-sectional SEM images of tensile-fractured specimens of the CG (upper one) and bimodal (lower one) Al-Mg alloys. Arrows indicated the extrusion and tensile directions.

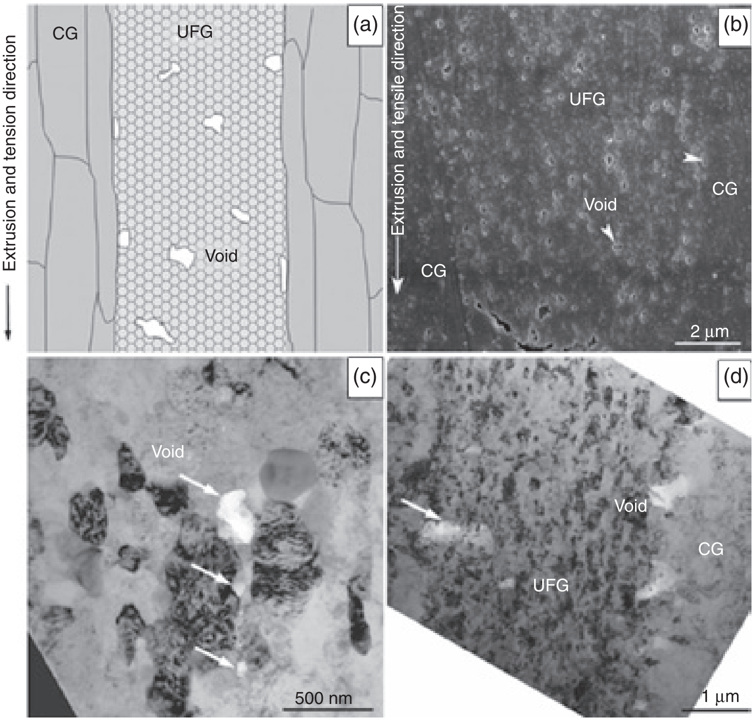

13.22 Void initiation in (a) schematic, (b) SEM and (c, d) TEM images.[30]

The fracture surface cross-section of the bimodal sample shows a mixed fracture mode: large shear lips with a flat central region. Scanning electron microscopy (SEM) revealed that voids near the tensile fracture surfaces tended to initiate both in the UFG matrix as well as at the UFG and CG interfaces (Fig. 13.22 (b)).

TEM observations further revealed small voids of about 50 to 300 nm at the UFG region and at the interface of CG and UFG regions (Fig. 13.22 (c, d)). Lee *et al.*[30] explained the above results as follows. Under tensile loading, the constrained ductile CG regions first undergo yielding and plastically deformed without fracture while the UFG matrix carried most of the tensile load elastically.[105] As the load continued to increase, the strong UFG regions plastically deformed very briefly after yielding at a higher stress. The stress concentration in the UFG matrix due to yielding may be relaxed by void generation and growth and by transferring local loads to the softer CG regions. Moreover, the stress mismatch between the UFG and CG regions also increases with increasing quasi-static loading[105] and leads to initiation of interfacial voids.

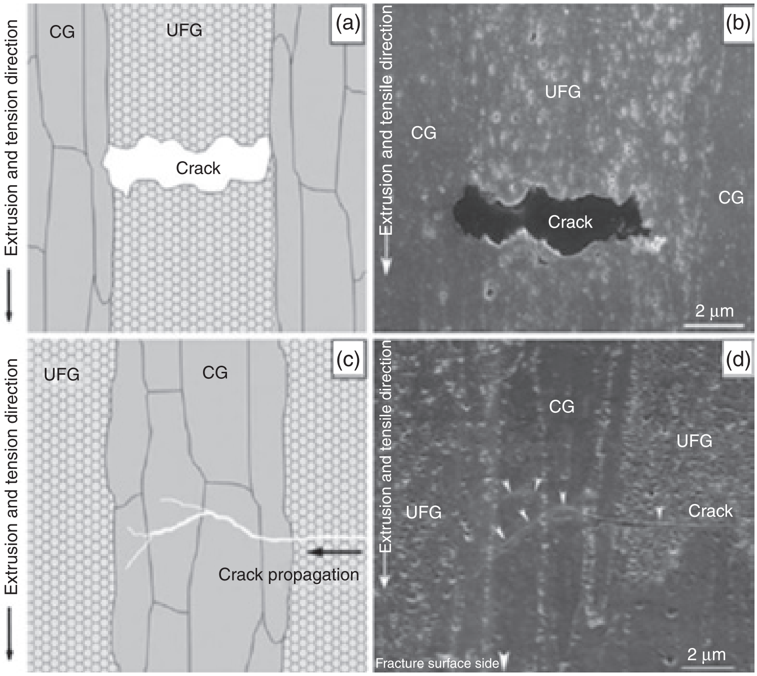

13.23 (a, b) Schematic and SEM micrograph of crack blunting of the UFG at the CG region. (c, d) Deflecting and branching of a longitudinal crack in CG by schematic and SEM image.[30]

Lee *et al.*[30] also observed evident cracks in the UFG 5083 matrix which were apparently arrested by the ductile CG regions. Figure 13.23 (a, b) shows a schematic of the crack blunting mechanism together with an SEM image of a similarly blunted crack in the UFG matrix sandwiched by CG bands. Figure 13.23 (c) shows a schematic of a crack that grew into a CG region, branched, and then stopped. A similar crack configuration was observed by SEM (Fig. 13.23 (d)).

These results indicate that crack propagation in the UFG regions tend to arrest at the CG regions, and interface voids appear to coalesce by transgranular-shear type separation and remain in the UFG regions. The ductile CG region may sustain additional plastic deformation beyond that of the UFG regions. Figure 13.24 (a, b) illustrates a process by which CG bands can bridge cracks and inhibit abrupt fracture. Note also that interface delamination between UFG and CG regions perpendicular to the fracture plane is evident in Fig. 13.24 (c, d) at the regions near fractures. These results suggest that large deformation occurs at the interface during crack nucleation and propagation. In addition, the necking deformation and dimple morphology that are also observed in the CG regions

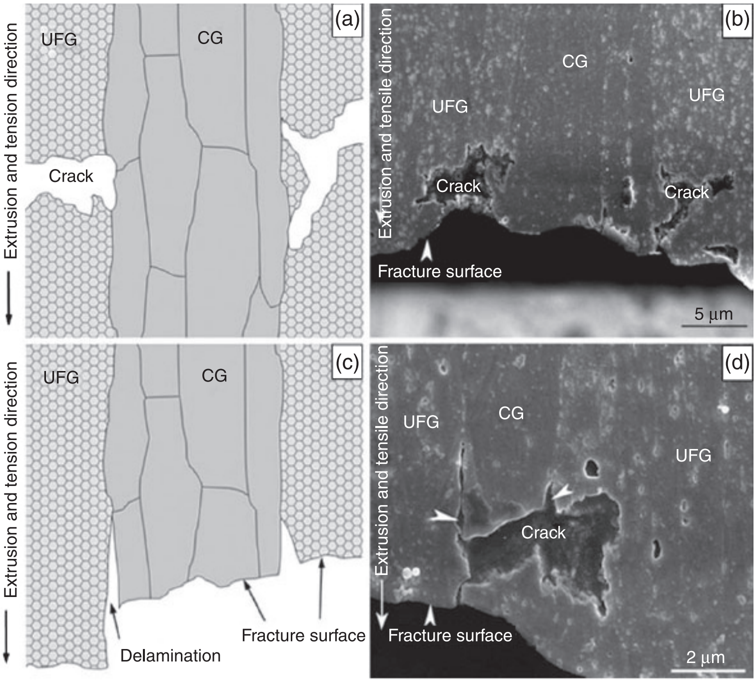

13.24 (a, b) Schematic and SEM image of crack bridging and branching of CG. (c, d) Interface delaminating and extensive plastic deformation of CG.[30]

indicate significant deformation in the CG regions via a ductile bridging mechanism (Fig. 13.25).[48]

Compression

Billard *et al.*[18] performed a careful investigation on deformation and fracture mechanisms of bimodal Al under compression. The fully dense bimodal Al was prepared by hot isostatic pressing of commercial purity Al nano-powders at 550°C under a pressure of 200 MPa for 600 min. As shown in Fig. 13.26, a proportion of microcrystalline grains (>1 μm) are embedded in UFG matrix with a mean grain size of 150 nm. Some of the CGs contain few dislocations (d) and/or a fine dispersion of γ-Al_2O_3 (p). Room temperature compressive testing, as shown in Fig. 13.27, revealed the high yield strength of 440 MPa and a total strain of 20%. Contrasting with the large strain hardening in bimodal Cu as observed by Wang *et al.*,[17] a very short strain hardening followed the elastic domain, then a plateau of the stress can be seen and is subsequently followed by linear work softening (beginning at 10% of true strain).

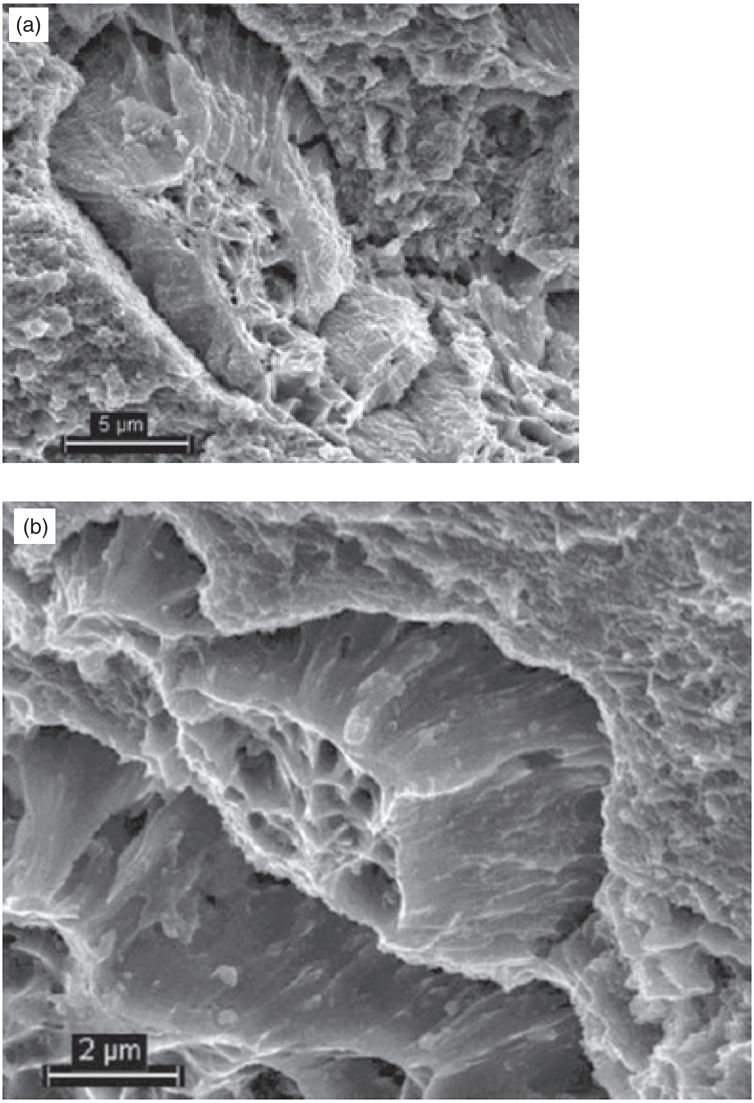

13.25 Fractography of the bimodal Al-Mg alloys with (a) 15% and (b) 30% volume fraction of CGs.[48]

After mechanical testing, one main crack appears, forming an angle of 45° ± 10° with the compression axis (Fig. 13.28). Some coarse grains have been intersected by the crack and these grains act as blunting obstacles, which provide support to the explanation on the improved ductility by CGs by Lee *et al.*[30]

Careful observation on the CGs revealed one or two slip systems, depending on the grain orientation (Fig. 13.28 (b)). This result illustrates an intense

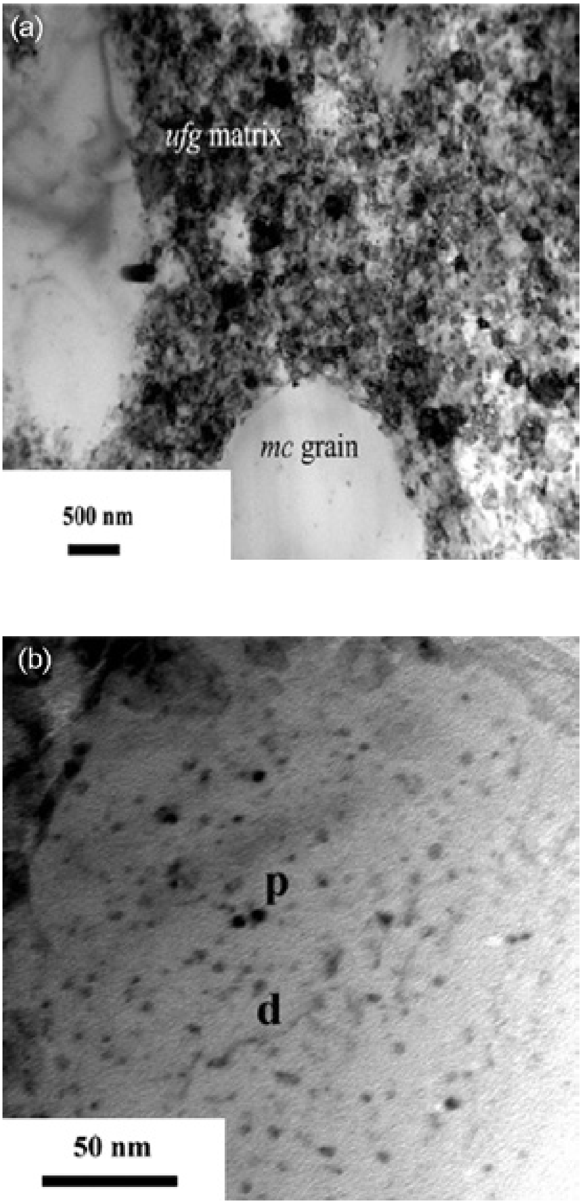

13.26 Bright-field TEM images showing (a) micrometer-sized (mc) grains embedded in UFG matrix and (b) one mc grain containing a fine dispersion of second-phase particles (p) and individual dislocations (d) that are pinned by the dispersoids.[18]

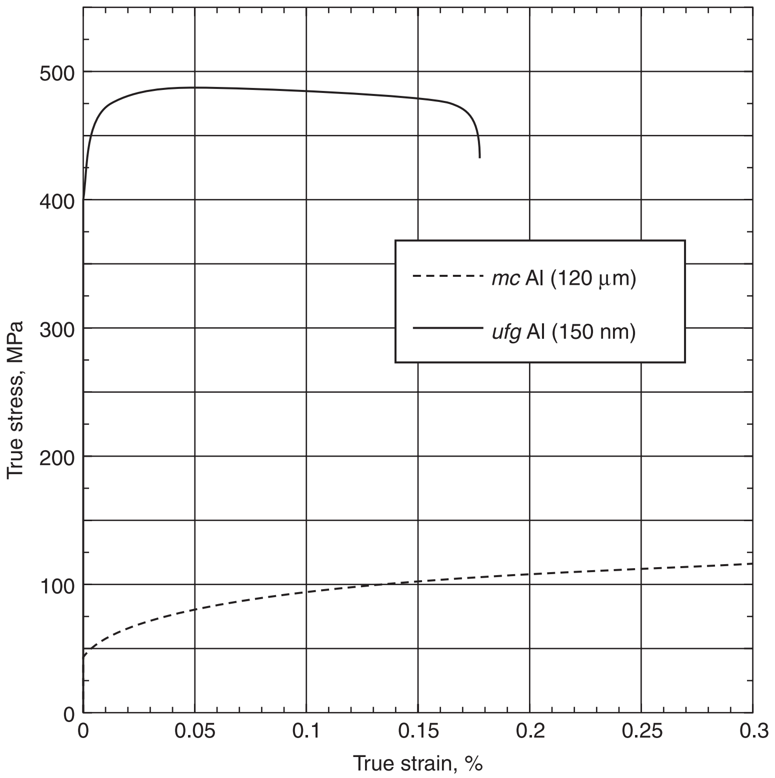

13.27 True stress–strain curves of both bimodal (ufg Al) and mc Al tested at room temperature by compression.[18]

plasticity-based dislocation activity inside the CGs. Post-mortem TEM observation further revealed that the CGs without the fine oxide dispersion were subdivided into equiaxed subgrains delimited by dense dislocation walls (Fig. 13.29 (a)).

The subgrain interior is dislocation free, suggesting the occurrence of a dynamic reorganization process. This dislocation arrangement is typical of high stacking fault energy face-centered cubic metallic materials, which were subjected to large-scale deformation.[106] For the CGs containing a fine dispersion of oxide phases, dislocations were pinned by obstacles and in some cases cut through by leaving small loops (Fig. 13.29 (b)). Twinning was not observed in the deformed CGs. As for the UFG matrix, deformation occurs within 'band' that are homogeneously distributed throughout the matrix (Fig. 13.30 (a)). Figure 13.30 (b) is a closer view of a band in the deformed UFG matrix by atomic force microscopy (AFM) technique. The traces of the two band systems are oriented at 55° and 60° to the compression axis. These features were interpreted as large groups of grains that are emerging from inside the sample, and roughly oriented along planes of

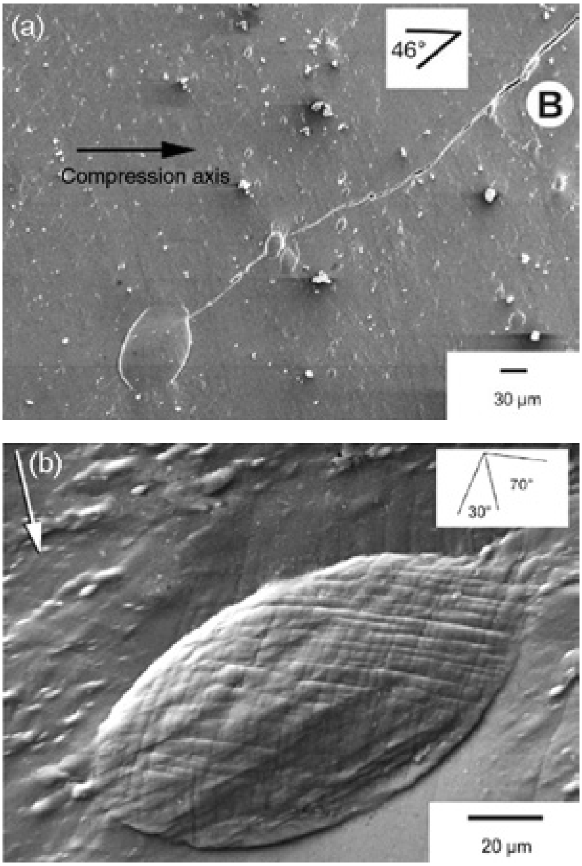

13.28 SEM images of the surface of bimodal Al compressive specimen showing (a) a primary crack (B) stopped by a CG grain, and (b) multiple slip in a large grain as a consequence of extensive dislocation activity.[18]

maximum shear.[18] Similar deformation shear bands were reported by Fan *et al.*[28] in a study involving compression testing of a bimodal Al-Mg alloy.

The above experimental and numerical results provide some insight into the deformation and fracture mechanisms that are activated in both UFG and CG regions, as well as UFG/CG interfaces of bimodal metallic materials, and reasonable explanations on both good and poor combinations of strength and ductility of bimodal metallic materials. Furthermore, they suggest that the factors required for attaining a combination of strength and ductility include: processing artifact-free metallic materials, uniform distribution of CGs in an UFG matrix, strong interfacial bonding between CG and UFG regions. However, inspection of the published literature also shows that systematic information on the precise mechanisms that govern microstructure evolution (such as grain orientation, for example) in the UFG region in bimodal metallic materials during large plastic

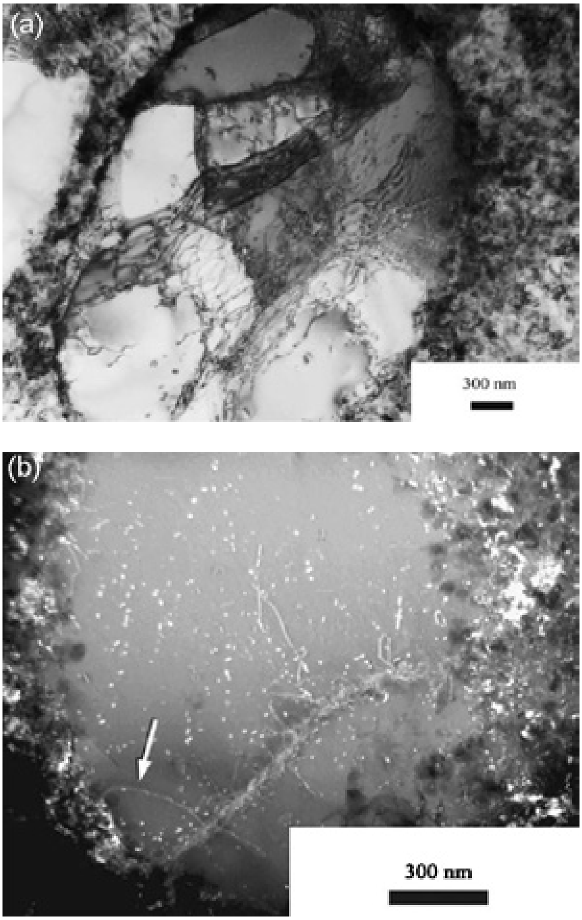

13.29 Post-mortem TEM images showing deformation microstructures of CGs embedded in the UFG matrix. (a) Dislocation-free cell, and (b) dislocation pinning (arrowed).[18]

deformation remain poorly understood. For example, key questions such as how is deformation in the UFG region related to plastic flow in the CG regions, will require additional experimental and theoretical studies.

13.3.3 Deformation and fracture mechanisms of multimodal metallic materials

Interestingly, there appears to be an almost complete absence of experimental studies focused on the deformation and fracture mechanisms that are active in multimodal metallic materials. There are, however, several numerical studies available, and these are discussed in the section that follows.

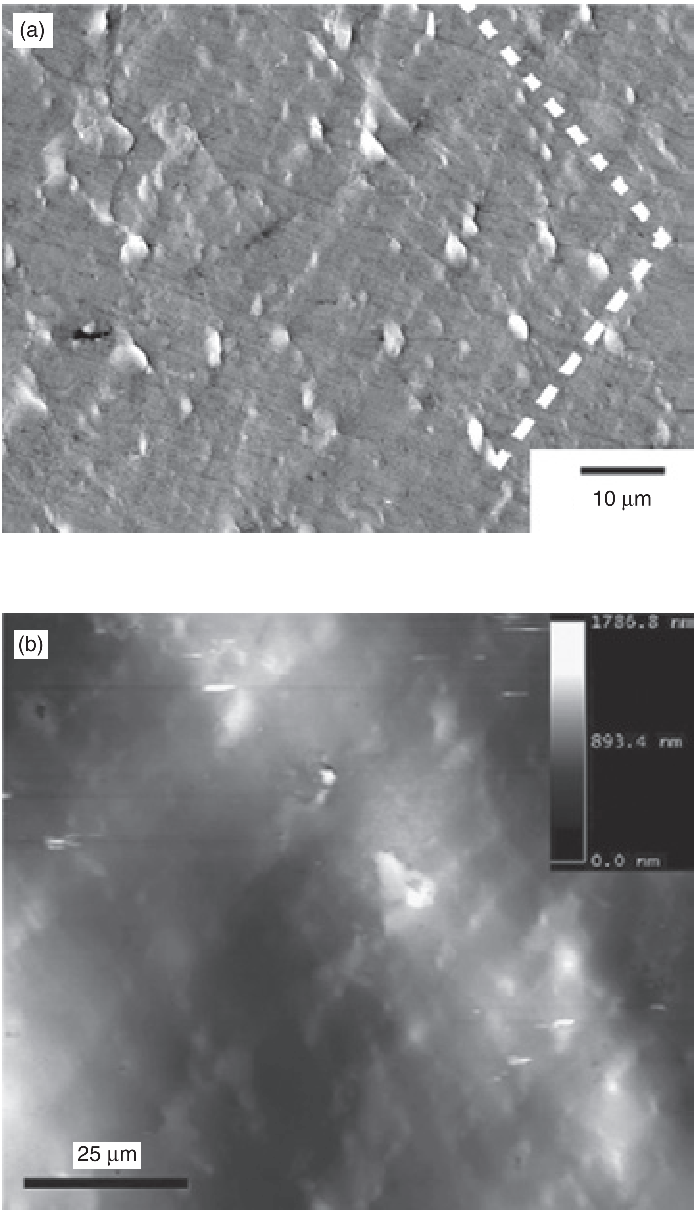

13.30 (a) SEM image showing deformation patterns of the UFG matrix after 20% compression strain. Two sets of symmetrical bands are visible and marked by dashed lines. (b) AFM topographic image of the surface of a deformed UFG matrix showing a 25 µm wide and stepped band.[18]

On the basis of a self-consistent approximation, Liu *et al.*[107] performed a numerical study on the deformation and fracture behavior of nanocrystalline metallic materials with a multi-scale grain size distribution. They generated the multi-scale metallic materials following a log-normal grain size distribution. The average grain size is 23 nm with a standard variation of 100. Figure 13.31 (a) shows the numerical results of local strain status less than 5% macroscopic strain.

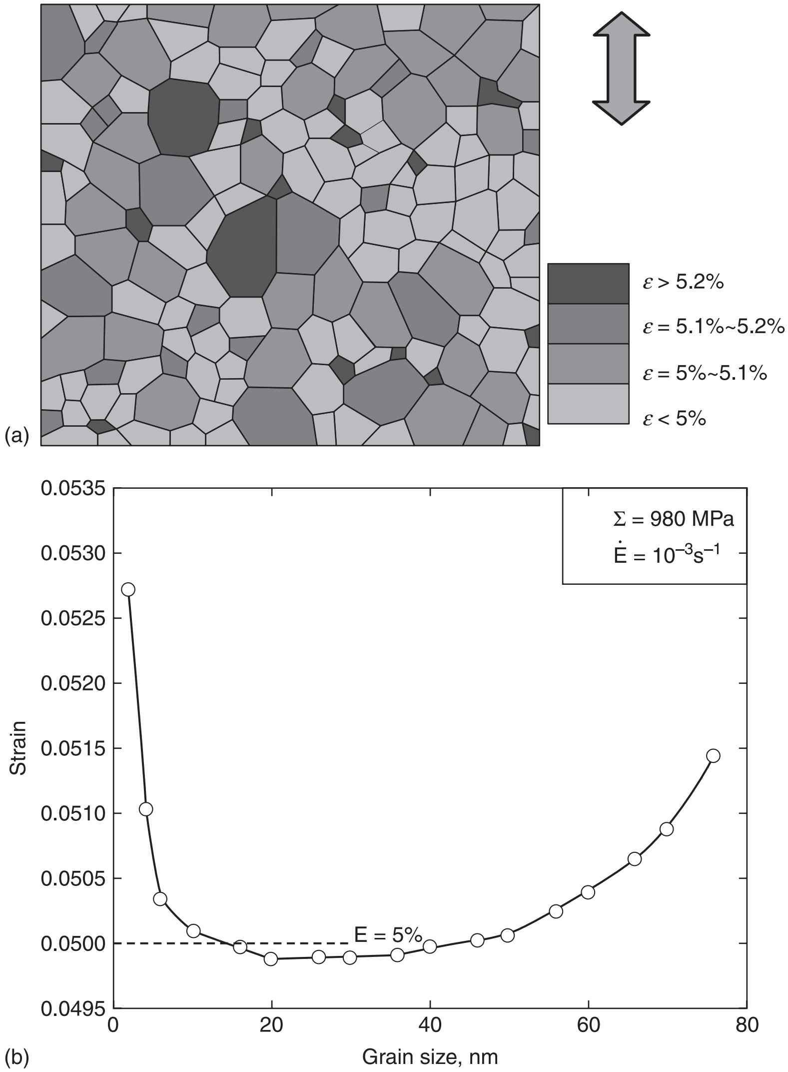

13.31 The status of local von Mises equivalent strains (a) and their grain size dependence (b) under uniaxial tensile at a macro von Mises equivalent strain of 5%.[107]

The local strains are grain size dependent, and they are non-uniform with various grain sizes. Figure 13.31 (b) shows the plastic strains (subjected to tension) of grains with different grain sizes under macroscopic strain rate of 10^{-3} s.$^{-1}$ It is evident that under these conditions plastic deformation of the multi-scale metallic materials is not homogeneous. The local strains of the grains smaller than 20 nm are higher than those corresponding to the overall grain size, indicating grain boundary mediated deformation mechanisms when the grain size decreases to a critical value. The local strain of grains larger than 40 nm increases with increasing grain size, and such an increasing tendency is consistent with the dislocation mediated deformation mechanisms that were discussed previously. Based on the theory that nanocracks nucleate at the interface between adjacent grains, Liu *et al.* explored the fracture behavior of multi-scale metallic materials. Figure 13.32 shows the behavior of fracture nucleation and plastic flow process under mechanical loading. During the early stages of loading, nanovoids are generated at the interface with relatively high local strains (a). With increasing plastic flow, more and more new nanovoids appear as a result of stress concentration. The initially formed nanovoids grow larger (b). The large nanovoids gradually transform into microvoids (c). At the same time, plastic flow is localized and gives rise to the necking formation (b and c). Subsequently, ductile fracture occurs through coalescence of microvoids (d).

In related numerical studies, Raeisinia *et al.*[55] comparatively studied the evolution of local strain and stress fields in UFG metallic materials with a mean grain size of 700 nm and different grain size distributions, and CG metallic materials with a mean of 10 μm and a wide grain size distribution, as shown in

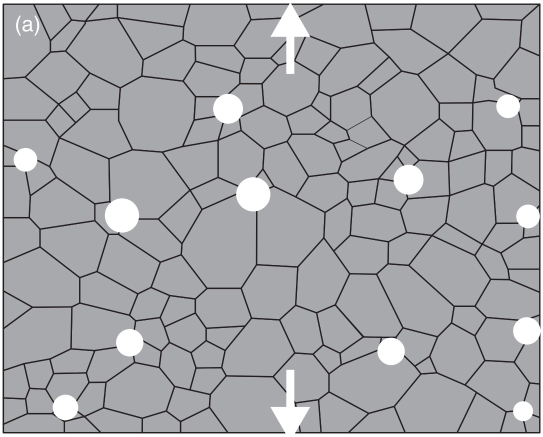

13.32 Predicted ductile fracture in nanocrystalline metallic materials with (a) formation of nanovoids (b) growing of nanovoids and formation of local necking with stress concentration (c) formation of microvoids (d) coalescence of microvoids.[107]

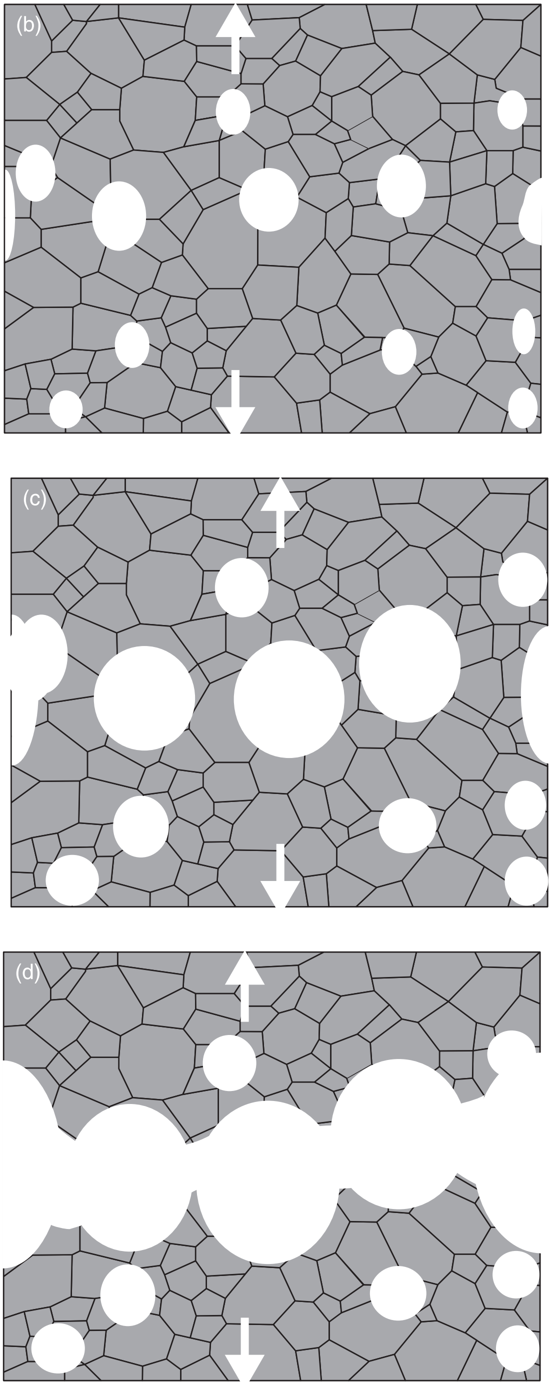

13.32 Continued.

Fig. 13.33. For these plots, the grains of each polycrystal were divided into size classes and the volume-weighted average of the equivalent stress and strain of the grains in each of these classes was calculated at different deformation steps.

The ratio of this value to the macroscopic equivalent stress and strain is plotted. The deformation of polycrystal with the narrow grain size distribution is more homogeneous, and this homogeneity increases as deformation progresses. The UFG grains of the polycrystal with wider grain size distribution tend to deform less and are under more stress than the average. As deformation advances, the polycrystals become less heterogeneous causing the strains and stresses in the grains to approach the far field average values. The polycrystal with the larger mean grain size loses this heterogeneity faster than the polycrystal with smaller mean grain size.

In summary, the above available numerical studies, despite their inherent assumptions and limitations, provide valuable insight into the deformation and fracture processes in multimodal metallic materials. That is, plastic deformation of the multimodal metallic materials is not homogeneous. In case of multimodal metallic materials with a mean grain size smaller than 100 nm, the local strains of both small and large grains are higher than those corresponding to medium-sized grains. In the case of multimodal metallic materials with a mean grain size larger

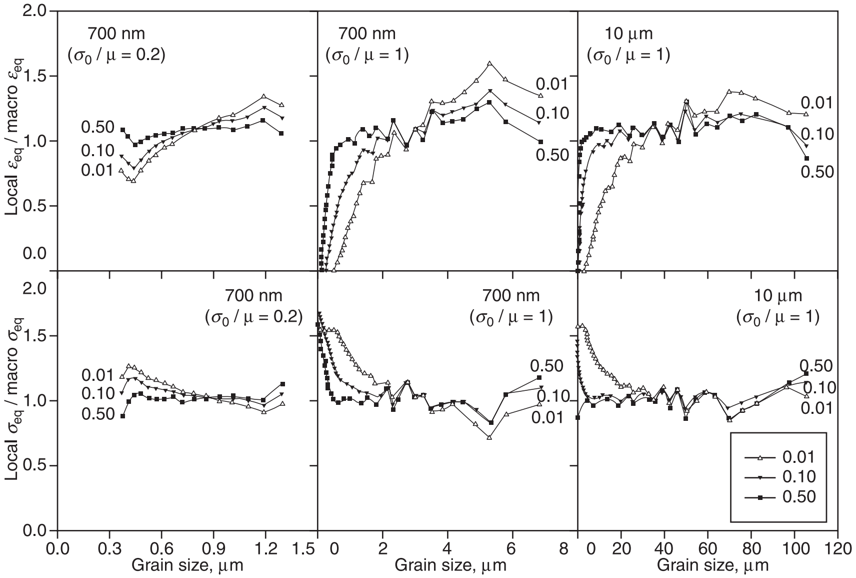

13.33 Predicted local relative von Mises equivalent stresses (bottom row) and strains (top row) as a function of grain size for three model polycrystals at three different stages of deformation corresponding to macro von Mises equivalent strain of 0.01, 0.10 and 0.50. The mean grain size and grain size distribution width (σ_0/μ) are indicated in the figures.[55]

than 100 nm, the small grains tend to deform less and are under more stress relative to the conditions experienced by the average-sized grains. Clearly, experimental studies that can provide some degree of experimental verification are needed.

13.4 Future trends

The discussion presented in the above sections confirms that, in terms of the strength–ductility space, both UFG and CG metallic materials are located at the two extreme poles, whereas multi-scale metallic materials tend to populate the central regime. Multi-scale metallic materials are of interest from both technological and fundamental perspectives. That is, in comparison with the behavior of unimodal UFG and CG metallic materials, multi-scale metallic materials offer improved combinations of strength and ductility and therefore, provide a pathway that should be exploited for technological applications that require toughness.

In comparison with UFG metallic materials with more than 30 years of history, multi-scale metallic materials represent a relatively new class, only approximately 10 years old. From a fundamental perspective, multi-scale metallic materials pose many interesting questions. For example, our knowledge of the mechanisms that govern the synthesis and behavior of multi-scale metallic materials is in its infancy, and phenomena such plasticity mechanisms, thermal stability, fatigue properties,[29,47,108] and dynamic properties of multi-scale metallic materials will require extensive additional studies.

13.5 Conclusions

Since initially reported in the year 2000, multi-scale grain size distributions are emerging as an effective strategy to improve the poor ductility of nanostructured and ultrafine-grained metallic materials. This chapter has mainly concentrated on mechanical behavior, deformation and fracture mechanisms of bulk multi-scale metallic materials. In addition, the chapter introduced the basic concepts, development background and history as well as preparation methods of multi-scale metallic materials in the introduction part. Finally the chapter discussed the potential technological implications and future investigations of this material.

Compared with unimodal ultrafine-grained and coarse-grained counterparts, multi-scale metallic materials (including bimodal and multimodal metallic materials) have a better combination of strength and ductility. If we designate the strength–ductility combination complying with the rule-of-mixtures as neutral combination, both positive (i.e. improved) and negative (i.e. diminished) deviations from the rule-of-mixtures have been reported experimentally for bimodal metallic materials, which might be caused by the inherent challenge to synthesize ideal samples that are defect-free and contain *a priori* design of multi-scale grain size distributions. Numerical studies on bimodal metallic materials predict both neutral and improved combination of strength and ductility, which can be attributed in part to the various assumptions made in the development of the numerical models. Therefore, systematic investigations are necessary to quantitatively reveal the mechanical properties and microstructure relationships of multi-scale metallic materials from both experiments and simulations.

The results of deformation and fracture mechanisms of bimodal metallic materials reasonably explained the positive and negative strength–ductility combinations. They also suggest that the factors required for attaining a balance of strength and ductility include: processing artifact-free metallic materials, uniform distribution of CGs in an UFG matrix, strong interfacial bonding between CG and UFG regions. However, systematic studies on the precise mechanisms that govern microstructure evolution in the UFG region in bimodal metallic materials during large plastic deformation are still necessary.

13.6 Acknowledgements

Y.H. Zhao and E.J. Lavernia would like to acknowledge supports by the Office of Naval Research (Grant number N00014-08-1-0370) with Dr. Lawrence Kabacoff as program officer, and the Army Research Laboratory (W911NF-08-2-0028).

13.7 References

1 Courtney T.H. Mechanical Behaviour of Materials, 1990; McGraw-Hill Companies, Inc.
2 Gleiter H. Prog Mater Sci 1989; 33: 223.
3 Valiev R.Z., Estrin Y., Horita Z., Langdon T.G., Zehetbauer M.J., Zhu Y.T. JOM 2006; 58(4): 33.
4 Meyers M.A., Mishra A., Benson D.J. Prog Mater Sci 2006; 51: 427.
5 Koch C.C., Morris D.G., Lu K., Inoue A. MRS Bull 1999; 24: 54.
6 Budrov Z., Swygenhoven H.V., Derlet P.M., Petegem S.V., Schmitt B. Science 2004; 304: 273.
7 Dieter G.E. Mechanical Metallurgy, 1988; McGraw-Hill Book Co., New York, pp. 289–290.
8 Koch C.C. Scripta Mater 2003; 49: 657.
9 Koch C.C., Youssef K.M., Scattergood R.O., Murty K.L. Adv Eng Mater 2005; 7: 787.
10 Ma E. Scripta Mater 2003; 49: 663.
11 Ma E. JOM 2006; 58(4): 49.
12 Zhao Y.H., Zhu Y.T., Lavernia E.J. Adv Eng Mater 2010, 12: 769.
13 Li Y.S., Zhang Y., Tao N.R., Lu K. Scripta Mater 2008; 59: 475.
14 Zhao Y.H., Topping T., Bingert J.F., Dangelewicz A.M., Li Y., Liu W., Zhu Y.T., Zhou Y.Z., Lavernia E.J. Adv Mater 2008; 20: 3028.
15 Legros M., Elliott B.R., Rittner M.N., Weertman J.R., Hemker K.J. Phil. Mag. A 2000; 80: 1017.
16 Tellkamp V.L., Melmed A., Lavernia E.J. Metall Mater Trans A 2001; 32: 2335.
17 Wang Y., Chen M., Zhou F., Ma E. Nature 2002; 419:912.

18 Billard S., Fondere J.P., Bacroix B., Dirras G.F. Acta Mater 2006; 54: 411.

19 Wu X., Xu W., Xia K. Mater Sci Eng A 2008; 493: 241.

20 Witkin D.B., Lee Z., Rodriguez R., Nutt S.R., Lavernia E.J. Scripta Mater 2003; 49: 297.

21 Lee Z., Rodriguez R., Hayes R.W., Lavernia E.J., Nutt S.R. Metall Mater Trans A 2003; 34: 1473.

22 Jin H., Lloyd D.J. Scripta Mater 2004; 50: 1319.

23 Lee Z., Witkin D.B., Radmilovic V., Lavernia E.J., Nutt S.R. Mater. Sci. Eng. A 2005; 410–411: 462.

24 Han B.Q., Mohamed F.A., Bampton C.C., Lavernia E.J. Metall Mater Trans A 2005; 36: 2081.

25 Han B.Q., Lee Z., Witkin D.B., Nutt S., Lavernia E.J. Metall Mater Trans A 2005; 36: 957.

26 Tang F., Hagiwara M., Schoenung J.M. Scripta Mater 2005; 53: 619.

27 Zhang Z.H., Han B.Q., Chung K.H., Lavernia E.J. Metall Mater Trans A 2006; 37: 2265.

28 Fan G.J., Choo H., Liaw P.K., Lavernia E.J. Acta Mater 2006; 54: 1759.

29 Walley J.L., Lavernia E.J., Gibelling J.C. Metall Mater Trans A 2009; 40: 2622.

30 Lee Z., Radmilovic V., Ahn B., Lavernia E.J., Nutt S.R. Metall Mater Trans A 2010; 41: 795.

31 Haouaoui M., Karaman I., Maier H.J., Hartwig K.T. Metall Mater Trans A 2004; 35: 2935.

32 Rabkin E., Gutman I., Kazakevich M., Buchman E., Gorni D.. Mater Sci Eng A 2005; 396: 11.

33 Das D., Samanta A., Chattopadhyay P.P. Synthesis and Reactivity in Inorganic, Metal-Organic and Nano-Metal Chemistry 2006; 36: 221.

34 Huang C.X., Wu S.D., Li G.Y., Li S.X. Mater Sci Eng A 2008; 483–484: 433.

35 Shekhar S., Cai J., Wang J., Shankar M.R. Mater Sci Eng A 2009; 527: 187.

36 Srinivasarao B., Oh-ishi K., Ohkubo T., Mukai T., Hono K. Scripta Mater 2008; 58: 759.

37 Zhao M.C., Yin F., Hanamura T., Nagai K., Atrens A. Scripta Mater 2007; 57: 857.

38 Zhao M.C., Hanamura T., Yin F., Qiu H., Nagai K. Metall Mater Trans A 2008; 39: 1691.

39 Chakrabarti D., Strangwood M., Davis C. Metall Mater Trans A 2009; 40: 780.

40 Azizi-Alizamini H., Militzer M., Poole W.J. Scripta Mater 2007; 57: 1065.

41 Wu S.J., Davis C.L. Mater Sci Eng A 2004; 387–389: 456.

42 Wang T.S., Zhang F.C., Zhang M., Lv B. Mater Sci Eng A 2008; 485: 456.

43 Lee T.R., Chang C.P., Kao P.W. Mater Sci Eng A 2005; 408: 131.

44 Shen X., Lian J., Jiang Z., Jiang Q. Mater Sci Eng A 2008; 487: 410.

45 Gubicza J., Bui H.Q., Fellah F., Dirras G.F. J Mater Res 1009; 24: 217.

46 Niendorf T., Canadinic D., Maier H.J., Karaman I. Scripta Mater 2009; 60: 344.

47 Sevillano J.G., Aldazabal J. Scripta Mater 2004; 51:795.

48 Ye R.Q., Han B.Q., Lavernia E.J. Metall Mater Trans A 2005; 36: 1833.

49 Joshi S.P., Ramesh K.T., Han B.Q., Lavernia E.J. Metall Mater Trans A 2006; 37: 2397.

50 Pozdnyakov V.A. Tech Phys Lett 2007; 33: 1004.

51 Berbenni S., Favier V., Berveiller M. Comp Mater Sci 2007; 39: 96.

52 Berbenni S., Favier V., Berveiller M. Inter J Plasticity 2007; 23: 114.

53 Malygin G.A. Phys Solid State 2008; 50: 1032.

54 Malygin G.A. Phys Solid State 2008; 50: 1056.
55 Raeisinia B., Sinclair C.W., Poole W.J., Tome C.N. Modelling Simul Mater Sci Eng 2008; 16: 025001.
56 Sano T., Rohrer G.S. J Am Ceram Soc 2007; 90: 211.
57 Laws V. J Mater Sci Lett 1983; 2: 527.
58 Prasad M.J.N.V., Suwas S., Chokshi A.H. Mater Sci Eng A 2009; 503: 86.
59 Valiev R.Z., Isamgaliev R.K., Alexandrov I.V. Prog Mater Sci 2000; 45: 103.
60 Kurzydlowski K.J. Scr Metall Mater 1990; 24: 879.
61 Morita T., Mitra R., Weertman J.R. Mater Trans 2004; 45: 502.
62 Zhu B., Asaro R.J., Krysl P., Zhang K., Weertman J.R. Acta Mater 2006;54: 3307.
63 Masumura R., Hazzledine P.M., Pande C.S. Acta Mater 1998; 46: 4527.
64 Phaniraj M.P., Prasad M.J.N.V., Chokshi A.H. Mater Sci Eng A 2007; 463: 231.
65 Chokshi A.H., Rosen A., Karch J., Gleiter H. Scripta Metall 1989; 23: 1679.
66 Shen T.D., Schwarz R.B., Feng S., Swadener J.G., Huang J.Y., Tang M., Zhang J., Vogel S.C., Zhao Y. Acta Mater 2007; 55: 5007.
67 Yamakov V., Wolf D., Phillpot S.R., Mukherjee A.K., Gleiter H. Nature Mater 2002; 1: 45.
68 Schiøtz J., Jacobsen K.W. Science 2003; 301: 1357.
69 Lu L., Chen X., Huang X., Lu K. Science 2009; 323: 607.
70 Cheng S., Spencer J.A., Milligan W.W. Acta Mater 2003; 51: 4505.
71 Swygenhoven H. Van, Derlet P.M.. Phys Rev B 2001; 64: 224105.
72 Moldovan D., Wolf D., Phillpot S.R. Acta Mater 2001; 49: 3521.
73 Swygenhoven H. Van. Science 2002; 296: 66.
74 Gutkin Y.M., Ovid'ko I.A., Skiba N.V. Acta Mater 2003; 51: 4059.
75 Shan Z., Stach E.A., Wiezorek J.M.K., Knapp J.A., Follstaedt D.M., Mao S.X. Science 2004; 305: 654.
76 Jin M., Minor A.M., Stach E.A., Morris J.W. Acta Mater 2004; 52: 5381.
77 Yamakov V., Wolf D., Phillpot S.R., Mukherjee A.K., Gleiter H. Nature Mater 2004; 3: 43.
78 Chinh N.Q., Szommer P., Horita Z., Langdon T.G. Adv Mater 2006; 18: 34.
79 Gianola D.S., Petegem S. Van, Legros M., Brandstetter S., Swygenhoven H. Van, Hemker K.J. Acta Mater 2006; 54: 2253.
80 Legros M., Gianola D.S., Hemker K.J. Acta Mater 2008; 56: 3380.
81 Wang Y.B., Li B.Q., Sui M.L., Mao S.X. Appl Phys Lett 2008; 92: 011903.
82 Wang Y.B., Ho J.C., Liao X.Z., Li H.Q., Ringer S.P., Zhu Y.T. Appl Phys Lett 2009; 94: 011908.
83 Rupert T.J., Gianola D.S., Gan Y., Hemker K.J. Science 2009; 326: 1686.
84 Cheng S., Zhao Y.H., Guo Y., Li Y., Wei Q., Wang X.L., Ren Y., Liaw P.K., Choo H., Lavernia E.J. Adv Mater 2009; 21: 5001.
85 Pan D., Kuwano S., Fujita T., Chen M.W. Nano Lett 2007; 7: 2108.
86 Zhao Y.H., Guo Y.Z., Wei Q., Dangelewicz A.M., Xu C., Zhu Y.T., Langdon T.G., Zhou Y.Z., Lavernia E.J. Scripta Mater 2008; 59: 627.
87 Zhao Y.H., Guo Y.Z., Wei Q., Troy T.D., Dangelewicz A.M., Zhu Y.T., Langdon T.G., Lavernia E.J. Mater Sci Eng A 2009; 525: 68.
88 Sergueeva A.V., Mukherjee A.K. Rev Adv Mater Sci 2006; 13: 1.
89 Sergueeva A.V., Mara N.A., Mukherjee A.K. J Mater Sci 2007; 42: 1433.
90 Sergueeva A.V., Mara N.A, Valiev R.Z., Mukherjee A.K. Mater Sci Eng A 2005; 410–411: 413.

91 Sabirov I., Estrin Y., Barnett M.R., Timokhina I., Hodgson P.D. Acta Mater 2008; 56: 2223.
92 Vinogradov A., Hashimoto S., Patlan V., Kitagawa K. Mater Sci Eng A 2001; 319–321: 862.
93 Liao X.Z., Zhao Y.H., Zhu Y.T., Valiev R.Z., Gunderov D.V. J Appl Phys 2004; 96: 636.
94 Liao X.Z., Zhao Y.H., Srinivasan S.G., Zhu Y.T., Valiev R.Z., Gunderov D.V. Appl Phys Lett 2004; 84: 592.
95 Wu X.L., Zhu Y.T. Appl Phys Lett 2006; 89: 3.
96 Wu X.L., Ma E. Appl Phys Lett 2006; 88: 3.
97 Wu X.L., Zhu Y.T. Phys Rev Lett 2008; 101: 4.
98 Kumar K.S., Suresh S., Chisholm M.F., Horton J.A., Wang P. Acta Mater 2003; 39: 3257.
99 Kumar K.S., Swygenhoven H. Van, Suresh S. Acta Mater 2003; 51: 5743.
100 Cheng S., Ma E., Wang Y.M., Kecskes L.J., Yousef K.M., Koch C.C., Trociewitz U.P., Han K. Acta Mater 2005; 53: 1521.
101 Yousef K.M., Scattergood R.O., Murty K.L., Koch C.C. Appl Phys Lett 2005; 87: 091904.
102 Ovid'ko I.A., Sheinerman A.G. Rev Adv Mater Sci 2007; 16: 1.
103 Zhao Y.H., Li Y., Topping T.D., Liao X.Z., Zhu Y.T., Valiev R.Z., Lavernia E.J. Int J Mater Res 2009; 100: 1647.
104 Gao H.J., Huang Y. J Mech Phys Solids 1999; 47: 1239.
105 Lee Z., Lee J., Lavernia E.J., Nutt S.R. MRS Symp Proc 2004; 821:9. 11.
106 Dirras G.F., Duval J.L., Swiatnicji W. Mater Sci Eng A 1999; 263: 85.
107 Liu Y.G., Zhou J.Q., Ling X. Mater Sci Eng A 2010; 527: 1719.
108 Simchi H., Simichi A. Mater Sci Eng A 2009; 507: 200.